ELEMENTA
Science of the Anthropocene

Engelhardt, V, et al. 2022. Black carbon and particulate matter mass concentrations in the Metropolitan District of Caracas, Venezuela. *Elem Sci Anth*, 10: 1. DOI: https://doi.org/10.1525/elementa.2022.00024

RESEARCH ARTICLE

# Black carbon and particulate matter mass concentrations in the Metropolitan District of Caracas, Venezuela: An assessment of temporal variation and contributing sources

Vanessa Engelhardt[1,2], Tibisay Pérez[1,3,*], Loreto Donoso[1], Thomas Müller[4], and Alfred Wiedensohler[4]

Atmospheric aerosols play an important role in atmospheric processes and human health. Characterizing atmospheric aerosols and identifying their sources in large cities is relevant to propose site-specific air pollution mitigation strategies. In this study, we measured the mass concentration of atmospheric aerosols with an aerodynamic diameter smaller than 2.5 μm ($PM_{2.5}$) in the city of Caracas (urban) and in a tropical montane cloud forest (suburban site, located in a mountainous area 11 km far from Caracas) between June 2018 and October 2019. We also measured equivalent black carbon (eBC) mass concentration in $PM_{2.5}$ in Caracas during the same period. Our goal is to assess $PM_{2.5}$ and eBC temporal variation and identify their major sources in the area. eBC showed a pronounced diurnal cycle in the urban site, mainly modulated by traffic circulation and the diurnal changes of the mixing layer height. In contrast, $PM_{2.5}$ showed stable median values during the day with slight variations like that of eBC. In the forest site, $PM_{2.5}$ values were higher in the afternoons due to the convective transport of aerosols from Caracas and other surrounding urban areas located in adjacent valleys. The annual median for eBC and $PM_{2.5}$ was 1.6 and 9.2 μg $m^{-3}$, respectively, in the urban site, while $PM_{2.5}$ in the forest site was 6.6 μg $m^{-3}$. To our knowledge, these are the first measurements of this type in the northernmost area of South America. eBC and $PM_{2.5}$ sources identification during wet and dry seasons was obtained by percentiles of the conditional bivariate probability function (CBPF). CBPF showed seasonal variations of eBC and $PM_{2.5}$ sources and that their contributions are higher during the dry season. Biomass burning events are a relevant contributing source of aerosols for both sites of measurements inferred by fire pixels from satellite data, the national fire department's statistics data, and backward trajectories. Our results indicate that biomass burning might affect the atmosphere on a regional scale, contribute to regional warming, and have implications for local and regional air quality and, therefore, human health.

**Keywords:** Black carbon, Latin America and the Caribbean, Air pollution, PM 2.5, Biomass burning, Caracas, Venezuela

## 1. Introduction

Atmospheric aerosols scatter and absorb solar and terrestrial radiation. They also participate in aerosol–cloud mechanisms because they act as cloud condensation nuclei. These interactions modify Earth's radiative forcing and, hence, alter the climate (Haywood, 2021). Radiative forcing estimates from atmospheric aerosols still present high uncertainties (Intergovernmental Panel on Climate Change [IPCC], 2021). Furthermore, exposure to atmospheric aerosols with an aerodynamic diameter smaller than 2.5 μm ($PM_{2.5}$) is considered to impact human health (Landrigan et al., 2018).

Air pollution affects more than 80% of the population in densely populated urban areas (Zhu et al., 2013). High $PM_{2.5}$ mass concentrations are characteristic in these sites due to traffic emissions, among other sources (Chen et al., 2016). A significant portion of $PM_{2.5}$ from traffic emissions is composed of black carbon. This type of aerosol is produced and emitted from the incomplete combustion of fossil fuels, biofuels, and biomass burning, and it is considered a short-lived climate pollutant (Andreae, 2001;

[1] Centro de Ciencias Atmosféricas y Biogeoquímica, Instituto Venezolano de Investigaciones Científicas, Caracas, Venezuela
[2] Atmospheric Chemistry Department, Leibniz Institute for Tropospheric Research, Leipzig, Germany
[3] Department of Environmental Science, Policy, and Management, University of California, Berkeley, CA, USA
[4] Department of Experimental Aerosol and Cloud Microphysics, Leibniz Institute for Tropospheric Research, Leipzig, Germany
* Corresponding author:
Email: tibisayperez@berkeley.edu

Bond et al., 2013). Additionally, black carbon aerosols have a fractal-like structure with a high surface area that adsorbs carcinogenic molecules of polycyclic aromatic hydrocarbons (Shrivastava et al., 2017).

Densely populated areas of developing countries experience rapid vehicle fleet growth (Wang et al., 2019). A significant portion of these vehicle fleets comprises old cars due to secondhand car importations from industrialized countries and inadequate air quality regulations (Wang and Yeo, 2016). Moreover, vehicles over 5 years in use are reported to have larger black carbon and $PM_{2.5}$ emission factors than newer vehicles. For instance, diesel and gasoline cars in use for less than 5 years have black carbon emission factors reduction by 60% and 47% from those in use for 5–10 years (Jezek et al., 2015). Therefore, old cars usage represents a technology that can significantly contribute to air pollution in low-income countries of South America. In particular, in Venezuela, most of the public transport (0.092 million vehicles) and cargo fleet (0.99 million vehicles) is made up of diesel-based engines (Instituto Nacional de Transporte Terrestre, 2013).

In the north of South America, aerosols derived from fossil fuel combustion, biomass burning, sea spray, and mineral dust are ubiquitous (Prospero, 1981; Sanhueza et al., 1987; Saturno, 2013; Morantes et al., 2021). Mineral dust from the Saharan desert in Africa can reach South America and intrude the mixing layers, contributing to significant effects on air quality, human health, and climate (Bozlaker et al., 2013; Prospero and Mayol, 2013; Kabatas et al., 2014). Mineral dust intrusions have been widely observed in Colombia (Ramirez, 2014), Puerto Rico (Colarco et al., 2003), Brazil (Gioda et al., 2011), Venezuela (Saturno, 2013; Morantes et al., 2021), and the Amazon Basin (Swap et al., 1992; Moran-Zuloaga et al., 2018), among other sites. Additionally, mineral dust from the Saharan desert can be enriched by biomass burning aerosols emitted and produced by the sub-Sahelian region in Africa (Salvador et al., 2016).

Forest fires are present throughout the north of South America due to land-use change and agricultural activities (Thornhill et al., 2018). The primary contributing source to biomass burning aerosol is the fires in Los Llanos region (Sanhueza et al., 1987). These events occur over the country and can experience long-range transport. A rise in biomass burning aerosols during the dry season has been reported at a high-altitude remote station (4,765 m.a.s.l.) in the lower free troposphere of the Andes region in Venezuela (Schmeissner et al., 2011; Hamburger et al., 2013).

Ground-based measurements of aerosol and short-lived climate pollutants are still scarce in the north of South America (Andrade-Flores et al., 2016). For the region, determining aerosol sources and their temporal variation is important because it can provide relevant information to improve air quality strategies, validate general circulation models' outputs and reduce the regional radiative forcing uncertainties (Riojas-Rodriguez et al., 2016; UNEP and CCAC, 2018). In the northernmost area of South America, particularly in Venezuela, the only air quality regulation regarding aerosol is total suspended particles, which have a diameter range of <50–100 μm (Ministerio del Ambiente y Recursos Naturales, 1995). Studies done in the region include $PM_{2.5}$ and elemental carbon measurements, among other variables, with offline instruments from samples collected with high-volume samplers (Sanhueza et al., 1987; Saturno, 2013). However, continuous measurements are needed to lead to a better temporal characterization in concentration and chemical composition and increase the understanding of aerosol regional transport.

In this work, we aim to fill that gap of information by measuring $PM_{2.5}$ and equivalent black carbon (eBC) by online instruments in Caracas and a tropical montane cloud forest in the city suburbs, with the following main objectives: (1) To evaluate diurnal, weekly, and seasonal variability of $PM_{2.5}$ and eBC, (2) to identify potential sources of $PM_{2.5}$ and eBC, and (3) to infer the local and regional impacts with regard to air pollution and aerosol transport. This study is an essential contribution to reduce radiative forcing uncertainties and improving the existing air quality policies in the region, suggesting $PM_{2.5}$ and black carbon as better air quality suitable criteria than total suspended particles (Kutlar Joss et al., 2017).

## 2. Campaign setup

### *2.1. Sites description*

We established 2 sampling sites: the city of Caracas (in the following referred to as the urban site) located on the roof (approximately 20 m a.g.l.) of the general command building Generalisimo Francisco de Miranda Air Base. The second site is a suburban area in a tropical montane cloud forest near Caracas (referred to as forest site). The site is located at a station belonging to the Venezuelan Institute for Scientific Research (IVIC) at 10 m a.g.l. (**Figure 1**, **Table 1**).

The metropolitan area of Caracas (urban site) has a high population density (approximately 1,223.41 inhabitants $km^{-2}$) (Instituto Nacional de Estadísticas, 2012). It is located in a relatively small, elongated, and narrow mountain valley (approximately 800 $km^2$) in the central-north-coastal area of Venezuela. The Cordillera de la Costa mountain range (2,765 m.a.s.l., Naiguatá Peak) is located north and separates the city from the Caribbean Sea (about approximately 20 km). It experiences a well-defined dry (December–April) and wet (May–November) seasonality. Caracas encompasses the financial, commercial, and communications service center of the country. Urban land use has spread to the surrounding hills, with few industries in the valley (Sanhueza et al., 1982). It has a large vehicle fleet and, as commonly found in the developing world, it is very outdated. Most of the vehicles are gasoline-based fueled, while public transportation is diesel-based. Our sampling site in Caracas is located in the geographic center of Caracas on a flat plane. This location is representative of the background characteristics of the city. Large-scale meteorological conditions in the valley are dominated by trade winds coming from the NNE. Most of the day, Caracas has prevailing dispersion conditions,

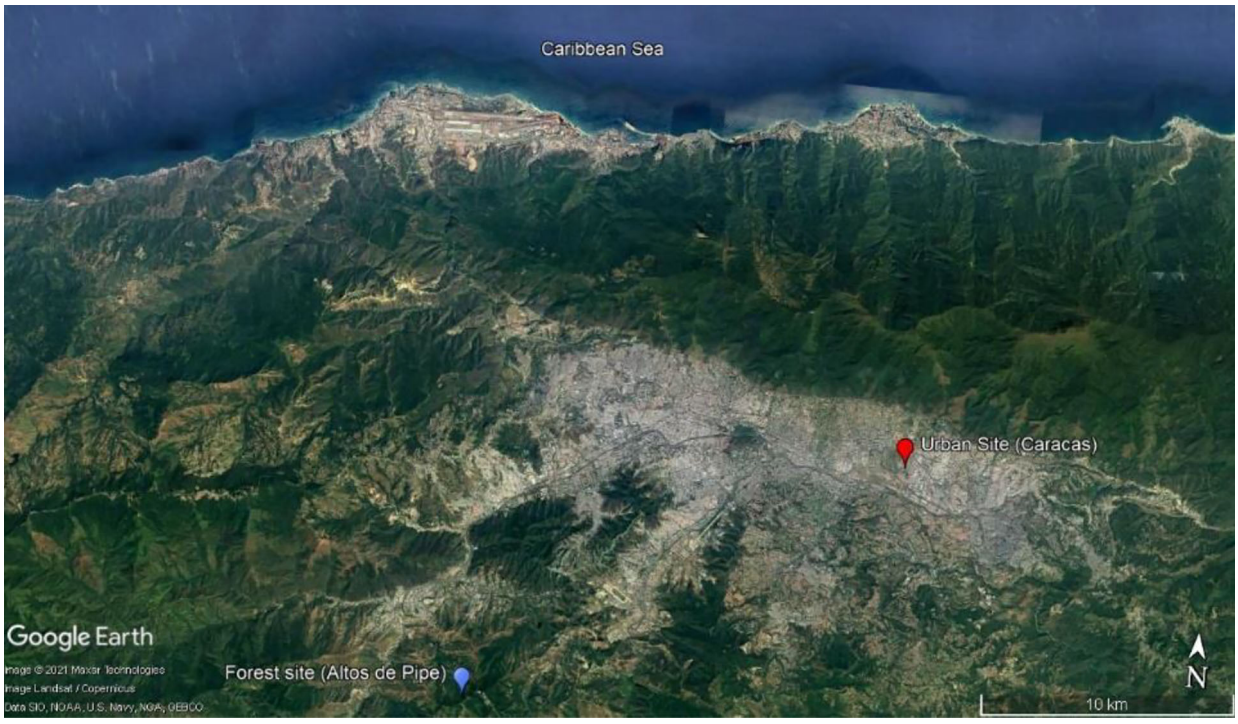


**Figure 1. Map of the Capital District of Venezuela in the North of South America.** Position of the urban site (Caracas) and the forest site (Altos de Pipe). The urban site is displayed as a red balloon, while the forest site as a blue balloon (Image © 2021 Maxar Technologies, Image Landsat/Copernicus).

**Table 1. Summary of the sampling sites description during the sampling period of this study**

| Site | Location | Geographic Coordinates | Type of Ecosystem | Altitude (m.a.s.l.) | Relative Humidity[a] ± *SD* (%) | Temperature[a] ± *SD* (°C) | Annual Precipitation[b] (mm) |
|---|---|---|---|---|---|---|---|
| Urban site | Caracas | 10°,49′N–66°,85′W | Mostly intervened | 900 | 77.4 ± 10.2 | 20.2 ± 3.2 | 912.8 |
| Forest site | Altos de Pipe | 10°,39′N–66°,99′W | Tropical mountainous and cloudy forest | 1,750 | 82.1 ± 11.5 | 16.8 ± 2.5 | 1,250 |

[a] Relative humidity and temperature values for the entire period of measurements ± (*SD*) standard deviation.

[b] Annual precipitation for 30 years reported for the site.

while temperature inversion forms at night, breaking up in the morning.

The valley has a tremendous dispersive capacity of gases and other pollutants, shown by a significant increase in the mixing layer height between 7:00 h and 9:00 h. (Sanhueza et al., 1982). Caracas mixing layer height average varies between 400 ± 230 m and 1190 ± 430 m, with an ascent rate of 395 ± 55 meters $h^{-1}$, equivalent to a 3.6 times dilution. The average mixing layer height from 9:00 h to 15:00 h ranges between 1927 and 2171 m. Later, after 16:00 h, the mixing layer's height decreases proportionally to the solar radiation intensity reduction (Figure S1; Sena, 2003). At this site, we measured eBC from June 2018 to October 2019, while $PM_{2.5}$ from December 2018 to November 2019.

The forest site is about 10 km away from Caracas. It is located in Altos de Pipe, a mountainous area in Miranda State (approximately 8.4 $km^2$), part of the Cordillera de la Costa mountain range. The main ecosystem is a tropical montane cloud forest with a well-defined dry (January–March) and wet (April–December) seasonality (**Table 1**). The annual temperature average is 17.6°C, the canopy of Altos de Pipe cloud forest ranges from 5 to 10 m., and the average relative humidity is 88%, which leads to the formation of mist with the rise of the moist air coming from the ocean (Cuenca, 1987; Sanhueza et al., 2000). Altos de Pipe is an excellent place to compare the atmospheric aerosols and trace gases concentrations with those found in Caracas due to the valley-mountain atmospheric dispersion effect related to its higher altitude

(Sanhueza 2002). At this site, we measured $PM_{2.5}$ from June 2018 to June 2019.

#### 2.2.1. Measurements of $PM_{2.5}$ mass concentration

The $PM_{2.5}$ mass concentration was measured at a 5-min time resolution using a continuous analyzer SHARP "Synchronized Hybrid Ambient Real-time Particulate" (Thermo Fisher Scientific, Waltham, MA, USA, model 5030i) equipped with a $PM_{2.5}$ cut-off size inlet, at a flow rate of 16.67 L $min^{-1}$. At both stations, the instruments were inspected weekly. The inspection included visual checks whether all the instrumental components were switched on and working correctly. The flow rate was checked and calibrated monthly with a reference flowmeter. The instrument consists of an array that combines a nephelometer detector and a radiometer. A detailed description of this instrument can be found in Hsu et al. (2016). $PM_{2.5}$ mass concentration is obtained from the linear relationship between the intensity of monochromatic light scattering by aerosols that pass through a light beam of 880 nm (nephelometer detector) and the beta radiation attenuation by particles that are deposited on a glass fiber filter (radiometer).

$PM_{2.5}$ concentration is calculated based on the $PM_{2.5}$ concentration average obtained by the nephelometer ($N_{\text{average}}$) and the ratio of $PM_{2.5}$ concentrations obtained between the radiometer and the nephelometer ($B/N$), which is considered a correction factor Equation 1,

$$\mathrm{PM}_{2.5}(\mu g\, m^{-3}) = N_{\text{average}} \times (B/N). \quad (1)$$

The coefficient of the light scattering signal was a parameter set by the manufacturer, while the time constant in $B/N$ was set for 20 min following the manufacturer's recommendations (Thomas and Gebhart, 1994; Gebhart, 2001; Hsu et al., 2016). The concentration of particles is proportional to the intensity of light scattering by particles with the same size distribution and chemical composition (Gebhart, 2001; Wang et al., 2009). Therefore, $PM_{2.5}$ concentration from the nephelometer is calculated from the relationship between the scattered intensity detected by the detector ($P$), the incident intensity ($I_o$), the detection volume ($V_m$), the total concentration of the number of particles ($C_n$), the particle number size distribution ($f(d_p)$), with $d_p$ (particle diameter), the integrated light scattering phase function for the corresponding solid angle ($S$), the wavelength ($\lambda$), and the refractive index ($m$) (Thomas and Gebhart, 1994; Gebhart, 2001; Hsu et al., 2016) (Equation 2),

$$P = I_o\, V_m\, C_n \int_o^{\infty} f(d_p) S(d_p, \lambda,\, m) \mathrm{d}d_p. \quad (2)$$

In the radiometer, the attenuation of beta radiation ($\beta^-$) is analyzed when radiation (electrons) passes through a layer of particles suspended in the filter and is related to the concentration of $PM_{2.5}$ by Equation 3, where $\beta$ is the electron flow transmitted, $\beta_o$ is the electron flow incident in the sample, $\mu$ is the attenuation coefficient (dependent on the energy of the beta radiation source, $^{14}$C) ($cm^2 g^{-1}$), and $x$ is the concentration of the particles ($g cm^{-2}$). $\mu$ value is determined by comparing standards of known mass with $\beta$ by the manufacturer (Kulkarni et al., 2011),

$$\beta = \beta_o e^{(-\mu x)}. \quad (3)$$

The instrument is calibrated with typical $PM_{2.5}$ aerosols standard compared to gravimetric reference methods (Jaklevic et al., 1981; Hsu et al., 2016). The sensitivity of the nephelometer depends on the particle size; therefore, the contributions of ultra-fine (Dp < 0.1 μm) and coarse (Dp > 2.5 μm) particles are underestimated. Particles larger than 2.5 μm size are underestimated since the mass scattering coefficients decrease with size, while ultra-fine particles are underestimated because they are within the Rayleigh scattering regime. The nephelometer automatically performs a zero in the measurement every 24 h to ensure the sensitivity of SHARP by circulating particle-free air after passing through a high-efficiency particulate air filter. On the other hand, the radiometer is automatically calibrated during the operation of the SHARP.

The $PM_{2.5}$ measurements usually have deviations related to the condensation of the water vapor in the filter, commonly contained in the sample flow of air mass entering the instrument. To reduce this interference, SHARP is equipped with a heating system that turns on automatically when the relative humidity exceeds 35%. Therefore, when heating the sample, it is not possible to discard volatile organic compounds lost due to evaporation (GAW Report No. 227, 2016). Nevertheless, it was reported that the loss of volatile organic compounds in the SHARP is lower compared to other instruments that use reference techniques to determine $PM_{2.5,}$ such as tapered element oscillating microbalance (Hsu et al., 2016). The SHARP fiberglass filter changed automatically every 24 h at midnight or when a saturation mass of 1500 μg was achieved in the filter.

#### 2.2.2. Measurements of equivalent black carbon mass concentrations in $PM_{2.5}$

The concentration of black carbon in $PM_{2.5}$ is derived from the measurement of the absorption coefficient ($C_{\text{abs}}$) at 1-min time resolution, obtained from the amount of light that is transmitted through a fiberglass filter loaded with aerosol particles using a multi-angle absorption photometer (MAAP) (Thermo Fisher Scientific, Waltham, MA, USA) (Petzold and Schönlinner, 2004). The instrument was equipped with a $PM_{2.5}$ cut-off size inlet and used at a flow rate of 16.67 l $min^{-1}$, checked, and calibrated monthly with a reference flowmeter. The MAAP automatically transforms the $C_{\text{abs}}$ into black carbon mass concentration, from the relationship between the $C_{\text{abs}}$ with the mass absorption cross-section of black carbon at 637 ± 1 nm, which is the operational wavelength of the MAAP. The instrument firmware uses a mass absorption cross-section value of 6.6 $m^2$ $g^{-1}$, the reference value used worldwide for rural and urban aerosols obtained during instrumental comparisons with a thermal reference method. For more information regarding the method, please visit Müller et al. (2011).

MAAP is considered the most sophisticated between the instruments that measure since it measures both the light transmittance in the orthogonal direction through the filter and the reflectance at 2 different angles, considering the effects of multiple light scattering and attenuation (Petzold and Schönlinner, 2004). This fact makes it more accurate than others and more consistent with the reference method (Petzold et al., 2005; Slowik et al., 2007; Moosmüller et al., 2009). In addition to this, the MAAP has a high time resolution (1 min), which allows daytime variability and rapid changes in environmental concentrations to be observed.

When using data derived from optical absorption methods, such as those obtained with the MAAP, to determine the concentration of black carbon, it is recommended to report these results as eBC concentration. In this way, the ambiguities in the literature are reduced, and it is also assumed that the concentration of eBC is equal to the concentration of elemental carbon measured by thermo-optical methods (Petzold et al., 2013). Therefore, we adopted the eBC terminology for reporting black carbon in this study.

### 2.3. Data quality control and instrument calibration

The PM monitors methods calibrations (nephelometer and radiometer) were done at the laboratory prior to the campaign at IVIC institute following the procedure in the instruction manual for the instrument model 5030i SHARP. The radiometer was calibrated with a mass transfer standard foil from the Thermo Fisher Scientific. Checks and calibrations of volumetric flow, temperature, and RH were done once per month or when it was possible to visit the sampling station. The photometer MAAP was calibrated at the TROPOS institute in Germany prior to the campaign in Venezuela. The data obtained from the instruments were checked and flagged, consisting of relative humidity of the sample above the recommended 35%, data below the detection limit, flow calibration periods, electricity shortage, and instrument failures. The dates and intervals for the data flagged and instrument calibration are available online (https://owncloud.gwdg.de/index.php/s/cidoBjSXbN8u8xA).

### 2.4. Meteorology, satellite products, and supplementary data

Local meteorology parameters with 5 min resolution were monitored at both sites, approximately 3 m far from each sampling station, including wind speed and direction, temperature, pressure, and relative humidity. The meteorological station used in the urban site was a Campbell Scientific USA, model WxPRO Entry-Level Research-Grade Weather Station, equipped with a Wind Monitor model 05103. In contrast, in the forest site, the meteorological station was a Davis brand Vantage Pro2 model 6152. Back trajectories were performed by the Hybrid Single-Particle Lagrangian Integrated Trajectory model (HYSPLIT, http://www.hysplit.uhu.es/hysplitweb08/HYSPLIT_traj.php; Draxler and Hess, 1988). Trade winds air masses from the North Atlantic are predominant during the year at both sampling sites. During September–October–November, the stations frequently receive air masses from the Caribbean Sea and air below 1,000 m of altitude from the southeast, presumed to be mostly continental air. Active fire locations from the Fire Information for Resource Management System (FIRMS) MCD14ML fire database (available online at https://earthdata.nasa.gov/active-firedata) were used to determine biomass burning events around the study sites. This information was complemented using the statistics of fire events reported from the firefighter department of the National Parks Institute (INPARQUES, Instituto Nacional de Parques).

### 2.5. eBC and $PM_{2.5}$ temporal variability, contributing sources, and statistical analysis

Time series and univariate analysis (i.e., mean, median, and 15th, 25th, 75th, and 85th percentiles), were used to infer the temporal variability of eBC and $PM_{2.5}$. We performed analysis of variance analysis for mean comparison among groups, and statistical significance with a $P$ value of $<0.05$ was determined. Data are presented as mean and standard deviation. The contribution of local sources to eBC and $PM_{2.5}$ was studied using the conditional bivariate probability function (CBPF) by percentiles. A summary of the measurement interval and the number of data points used to generate polar plots for the CBPF are described in Table S1. A complete description of the CBPF methodology can be found in Uria-Tellaetxe and Carslaw (2014). The function calculates the probability that a specific concentration of a particular pollutant is found in a specific wind vector. CBPF is plotted on bivariate polar graphs. In this way, clear contributions from pollutant sources based on wind vectors can be visualized.

CBPF uses wind speed as a third variable plotted on the radial axis and assigns percentile ranges of the pollutant concentration to wind speed and direction intervals. These CBPF ranges allow the identification of pollutant sources more rigorously because the sources tend to occupy precise concentration intervals. This characteristic of the sources is revealed because they tend to have a relatively constant emission rate. For example, high concentrations under low wind speeds ($<3$ m s$^{-1}$) indicate surface emissions released with little or no buoyancy. In contrast, high concentrations at high wind speeds ($>6$ m s$^{-1}$) are indicative of emissions at high velocity and a greater distance (Uria-Tellaetxe and Carslaw, 2014).

The function can be expressed by Equation 4, where $m_{\Delta\theta,\Delta u_{y\geq c\geq x}}$ is the number of pollutant samples in a wind vector $\Delta\theta$, with a speed interval of particular wind $\Delta\mu$, at a concentration range $c$, established by a range of percentiles $y - x$, and $n_{\Delta\theta,\,\Delta\mu}$ is the total number of samples present in a particular wind speed and direction interval,

$$\mathrm{CBPF}_{\Delta\theta,\Delta u} = \frac{m_{\Delta\theta,\Delta u_{y\geq c\geq x}}}{n_{\Delta\theta,\Delta u}}. \quad (4)$$

In the daily analysis of the time series, we noted occasions when high eBC and $PM_{2.5}$ mass concentrations persisted for some days during the dry season. We, therefore, deemed exploration of the circumstances surrounding these events. We reviewed whether air masses arriving at the forest and urban site during these high concentration

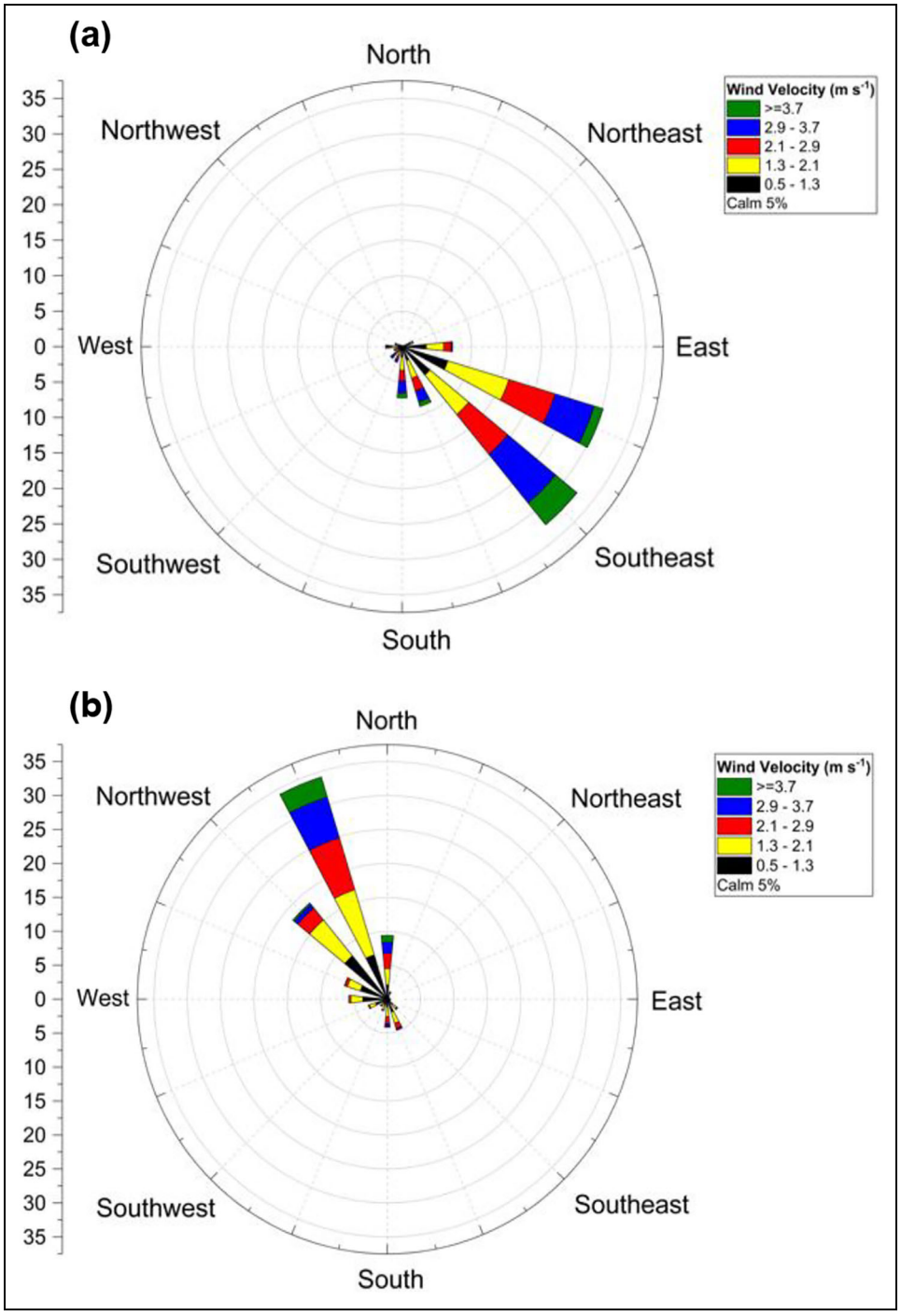


**Figure 2. Wind rose based on wind speed and direction hourly means at (a) the urban site and (b) the forest site (m $s^{-1}$).** The *y*-axis represents the sum of frequency percentages of wind velocities per wind direction bins.

events crossed fire regions, using the FIRMS database combined with HYSPLIT back-trajectories. For these particular events, the backward trajectories were calculated for 24 h duration, arriving every 6 h at every site, with altitudes of 1000 and 500 m.a.g.l.

## 3. Results

### *3.1. Meteorological parameters and $PM_{2.5}$ and eBC temporal variation*

Main meteorological parameters at both sites are typical of tropical regions (Table S2). Wind roses show that the prevailing wind direction is from the southeast and northwest vectors for the urban and forest sites, respectively (**Figure 2**). $PM_{2.5}$ and eBC means (from daily data) for the urban site were 11.9 ± 8.5 μg $m^{-3}$, and 1.8 ± 0.9 μg $m^{-3}$, respectively; while $PM_{2.5}$ for the forest site was 10.2 ± 9.8 μg $m^{-3}$ (**Figure 3**, **Table 2**). In the urban site, eBC to $PM_{2.5}$ ratio is 1:6, and $PM_{2.5}$ values were higher for the period of measurements than at the forest site.

$PM_{2.5}$ and eBC for the urban site and $PM_{2.5}$ for the forest site exhibited defined daily and seasonal cycles, higher during the dry season (December–May) (**Figures 3** and **4**).

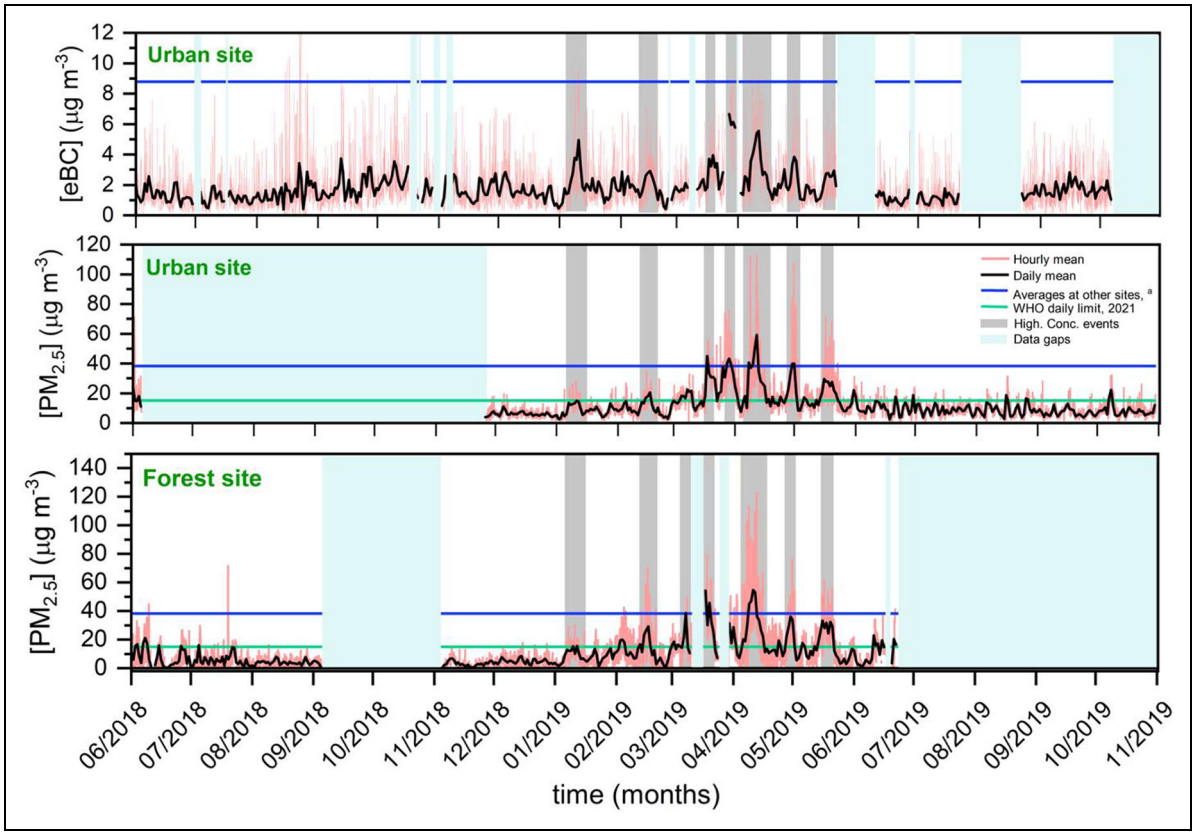


**Figure 3. Time series of $PM_{2.5}$ and eBC mass concentration in the urban and forest site (µg $m^{-3}$).** [a] References used to obtain the average $PM_{2.5}$ values from other sites: Sao Paulo, Brazil (Martins Pereira et al., 2017), Manila, Philipines (Cohen et al., 2009), San Juan, Puerto Rico (Figueroa et al., 2006), Lima, Perú (Silva et al., 2017), Hyderabad, India (Latha and Badarinath, 2005a), Maracaibo, Venezuela (Morales et al., 2012), Nueva Deli, India (Tiwari et al., 2013), Rio de Janeiro, Brazil (Mariani et al., 2007), Manaus, Amazonas, Brazil (Paralovo et al., 2019), Santiago de Chile, Chile (Koutrakis et al., 2005), Huancayo, Perú (Suárez-Salas et al., 2017), Ciudad de México, México (Amador-Muñoz et al., 2011), Buenos Aires, Argentina (Bogo et al., 2003), California, USA (Chow et al., 2006), Madrid, Spain and Londres, UK (Kassomenos et al., 2014), Taiwan, China (Cheng et al., 2000), Beijing, China (Liu et al., 2014), El Cairo, Egypt (Cheng et al., 2016). References used to obtain the eBC mean values from other sites: Sao Paulo, Brazil (Backman et al., 2012), Hyderabad and Telangana, India (Latha and Badarinath, 2005b), Dhaka, Bangladesh (Begum et al., 2012), Bangkok, Thailand (Sahu et al., 2011) Manila, Philipines (Alas et al., 2018), Anantapur, India (Kumar et al., 2011), Nueva Deli, India (Tiwari et al., 2013), Pune and Agra, India (Safai et al., 2007), Mumbai, India (Venkatraman et al., 2005), Guangzhou, China (Verma et al., 2010), Chennai, India (Aruna et al., 2013), Manaus, Amazonas, Brazil (Artaxo et al., 2002), New York, USA (Patel et al., 2009), Ciudad de Mexico, Mexico (Retama et al., 2015), Buenos Aires, Argentina (Resquin et al., 2018), Beijing, China (Liu et al., 2016).

In the urban area, eBC also displayed higher values during the dry season. Likewise, during the period of biomass burning in the dry season, we found higher eBC values in the urban site and $PM_{2.5}$ in both sites, in contrast to that of the rainy season ($P < 0.05$). For both sites, $PM_{2.5}$ mean values were larger during weekdays in comparison to weekends. The same is observed for eBC at the urban site (Table S3). During weekdays, the eBC diurnal cycle showed a maximum peak at 8:00 h., an absolute minimum at about 13:00 h, and a began rising again at 16:00 until about 21:00 h. Weekend patterns had the same trend but were flattened (**Figure 4**).

For the 7 days of the week, we determined daily hourly means of $PM_{2.5}$ and eBC concentrations in the urban site and $PM_{2.5}$ in the forest site during the biomass burning period in the dry and rainy seasons. A marked increment of eBC during the biomass burning period of approximately 30% higher is observed compared to the rainy season in the daily hour averages (**Figure 5**). The inter-hour variability of the eBC is bimodal, but with the highest concentration peak, between 17:00 h and 10:00 h, compared to what is observed for the rainy season and the entire sampling period.

### *3.2. CBPF applied to $PM_{2.5}$ and eBC mass concentrations*

The CBFP polar graphs for the concentrations of eBC and $PM_{2.5}$ for the urban site and $PM_{2.5}$ for the forest site showed seasonal patterns for different sources. For instance, during the wet season in the urban site, the CBPF for the percentiles 0–50th shows that the more probable eBC sources in the range of 0–1.1 µg $m^{-3}$ are

**Table 2. Summary of the median, average, standard deviation, and percentiles 25 and 75, for $PM_{2.5}$ and eBC for the entire period of measurements, from daily values, for the urban and forest site (μg $m^{-3}$)**

| Location | 25% | Median | Average | Standard Deviation | 75% |
|---|---|---|---|---|---|
| | | | (μg $m^{-3}$) | | |
| Urban site | | | | | |
| $PM_{2.5}$ | 6.45 | 9.17 | 11.91 | 8.54 | 13.71 |
| eBC | 1.17 | 1.55 | 1.75 | 0.89 | 2.08 |
| Forest site | | | | | |
| $PM_{2.5}$ | 3.71 | 6.63 | 10.23 | 9.78 | 13.63 |

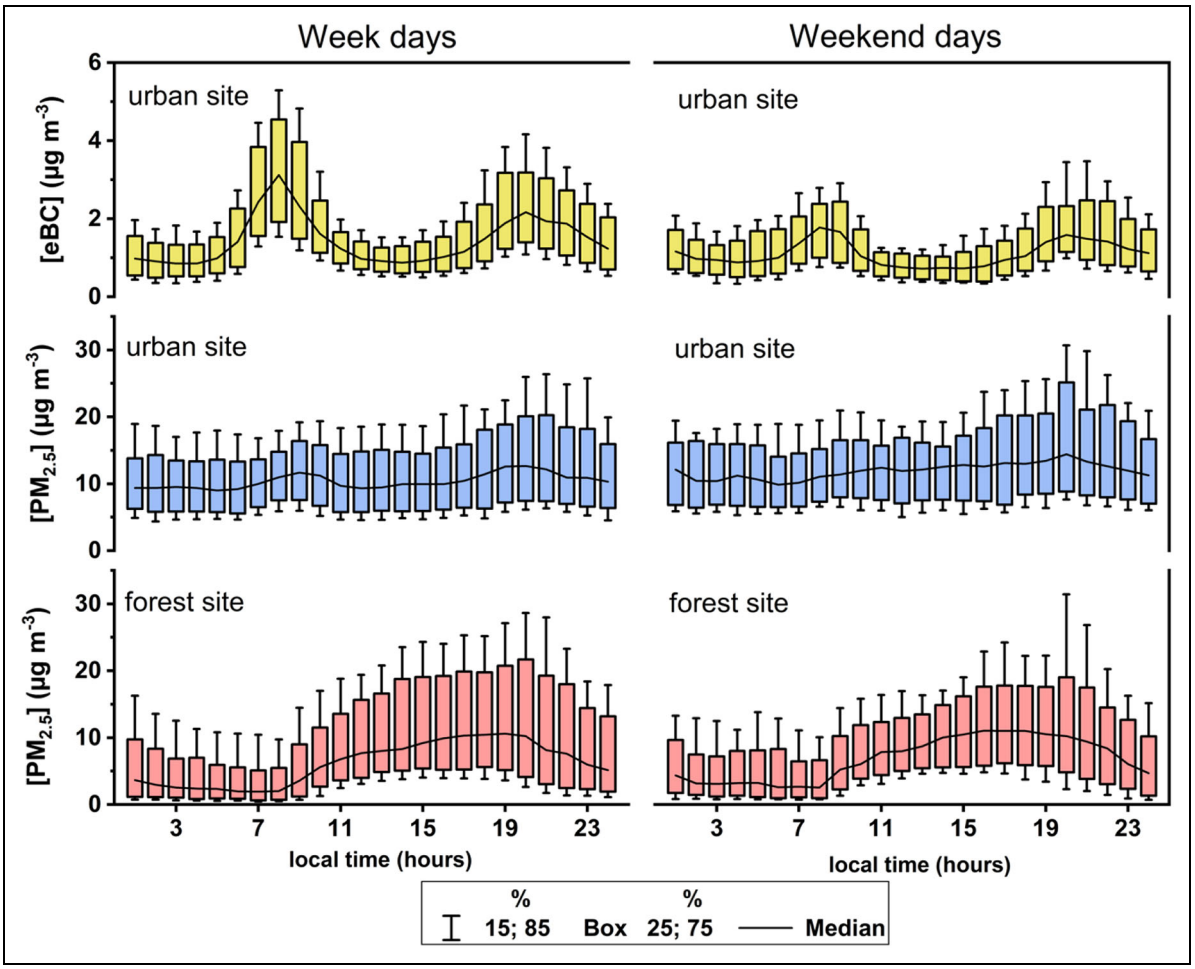


**Figure 4. Daily hour averages of eBC and $PM_{2.5}$ in μg $m^{-3}$ for the entire period of measurements, during weekdays and weekends.** Box border represents the 25th and 75th percentile, the gray whiskers represent the 15th and 85th percentile, and the line represents the median.

located in the southeast, with wind speeds below 5 m $s^{-1}$. Percentiles 50–100th of the CBPF show that eBC sources (1.1–9.5 μg $m^{-3}$) are spread within the northwest, southwest, and south, with wind speeds above 3 m $s^{-1}$ (**Figure 6**). During the dry season, the results for the percentiles 0–50th indicate that the more probable sources of eBC (0–1.5 μg $m^{-3}$) are in the southeast, and southwest, with wind speeds between 0 and 6 m $s^{-1}$. For the percentiles 50–100th, eBC sources (1.5–11 μg $m^{-3}$) are spread between the northwest, southwest, south, and southeast, with wind speed above 2 m $s^{-1}$ (**Figure 6c** and **d**).

Probable sources for $PM_{2.5}$ ($\leq$13 μg $m^{-3}$) in the urban site during the wet season are located in the north and west, with wind speed between 0 and 4 m $s^{-1}$. $PM_{2.5}$ sources for the percentiles 50–100th are found to the south and southeast, with wind speed >3 m $s^{-1}$ (Figure S2a and b). There is a specific contribution of $PM_{2.5}$ (0–9.7 μg $m^{-3}$) from the north and southeast during the dry season. For concentrations between 9.7 and 114 μg $m^{-3}$,

the sources are spread around the west, southwest, and southeast (Figures S2c and d). In the forest site, during the wet season, probable sources of $PM_{2.5}$ ($\leq$3.4 μg $m^{-3}$) are located at the north, with wind speed over 4 m $s^{-1}$. For concentrations between 3.4 and 63 μg $m^{-3}$, sources are mainly at the northwest (Figure S3a and b). During the dry season, probable $PM_{2.5}$ sources in the range of 0–8.5 μg $m^{-3}$ are shown in northwest and southwest directions, with wind speed (< 3 m $s^{-1}$). Sources of $PM_{2.5}$ with concentrations between 8.5 and 148 μg $m^{-3}$ have a very defined direction from the north, with wind speed over 3 m $s^{-1}$ (Figure S3c and d).

## 4. Discussion

### 4.1. $PM_{2.5}$ and eBC in the study sites and other locations

Mean daily values of eBC in the urban site was 1.75 ± 0.89 μg $m^{-3}$, while for $PM_{2.5}$ was 11.91 ± 8.54 μg $m^{-3}$, and 10.23 ± 9.78 μg $m^{-3}$ for the urban and forest site, respectively, for the entire period of measurements (**Table 2**). The eBC results of the present study are the first to be obtained with a high temporal resolution for the urban site (Caracas) and the country. eBC concentration in the urban site and $PM_{2.5}$ for both sites are low compared to typical average values from other urban areas (**Figure 3**).

High eBC and $PM_{2.5}$ concentrations would be expected given the large population density in Caracas metropolitan area (approximately 1223.41 inhabitants $km^{-2}$) (Instituto Nacional de Estadísticas, 2012) and its high vehicle fleet. Surprisingly, eBC and $PM_{2.5}$ concentrations values were low at both sites compared to the average from typical urban areas due to this region's particular meteorology, which prevents long residence time of the air masses. Every morning the planetary mixture layer breaks due to solar radiation, warming up the city surface. The warm and lower air masses expand as the atmosphere is heated from below and progressively warms the air above by convective heat transfer. This daily process releases the atmospheric aerosols and other trace gases air masses, resulting in a cleaner planetary mixture layer during the day, despite the large anthropic emissions from the surface (Sanhueza et al., 1982).

### 4.2. Diurnal cycle of $PM_{2.5}$ and eBC

The inter-hourly variability of eBC concentration is pronounced and bimodal. A high concentration peak occurs between 6:00 h and 8:00 h and one of lesser magnitude between 18:00 h and 22:00 h (**Figure 4**). The diurnal cycle of eBC during working days and weekends may be associated with fossil fuel combustion emissions from the highways traffic, which are characteristic of the urban site. Higher eBC concentrations in the early morning, reaching its peak at around 8:00 h, are caused by a large automobile traffic starting at 5:00 h (particularly public transportation, which is mostly diesel-based) and the lower mixing layer height. Later, at around 13:00 h, the observed decrease of eBC is caused by the fast dispersion of the pollutants and the dilution effect due to the maximum mixing layer height. Based on the wind roses (**Figure 2**), we can expect that these pollutants are transported at this time of the day, mainly to the forest site, located in the southwest of the urban site.

Previous studies have suggested that the valley might experience an increment in aerosol mass concentration and other pollutants every day after 16:00 h because of the reduction of the mixing layer height due to the temperature inversion (Sena, 2003). This effect encompasses the elevation in air temperature as altitude in the atmosphere increases, which prevents lower air masses from rising, then the air density is higher at lower altitudes (Seinfeld and Pandis, 1998; Finlayson-Pitts, 2000). Therefore, in this study, the high eBC concentration peak at 17:00 h, which kept increasing until about 20:00 h, can be explained by the temperature inversion in the Caracas valley at night. In the urban site, $PM_{2.5}$ mass concentration on weekdays and weekends exhibited minimal inter-hour changes, with slightly similar behavior to the observed for eBC. This behavior is mainly due to the difference in sources of $PM_{2.5}$ and eBC. While eBC comes mainly from fossil fuel combustion, $PM_{2.5}$ can be comprised of secondary organic aerosols derived from heterogeneous nighttime reactions (Liu et al., 2020; Liu et al., 2021). Therefore, this can be the most relevant $PM_{2.5}$ source at early hours, limiting us to distinguish the relative contribution of fossil fuel combustion.

In the forest site, there was a decrease in $PM_{2.5}$ from midnight until 7:00 h. Since the forest site is in a high mountainous area, the $PM_{2.5}$ concentrations found early in the morning represent the concentrations of the free troposphere, when the air mass of the city is confined in the valley due to the nocturnal inversion layer at a lower altitude. Therefore, the values measured in early hours at the forest site are considered the regional $PM_{2.5}$ background concentrations of the area. By that time, the median concentration was around 3 μg $m^{-3}$ for the entire period of measurements. Later, from 7:00 h to 20:00 h, the $PM_{2.5}$ concentration showed a progressive increment due to the expansion of the planetary boundary layer and possible transport of aerosol particles from other areas, including the urban site. This behavior is observed during weekdays and weekends, with the difference that the $PM_{2.5}$ mean is slightly lower on weekends.

### 4.3. Seasonal variation of $PM_{2.5}$ and eBC

Average concentrations of eBC in the urban site and $PM_{2.5}$ in both sites are higher during the dry season (**Figure 3**). An increase in aerosol mass concentration has been observed before within the mixing layer in different sites of Venezuela during the dry season (December–April) (Guajardo et al., 2010; Hamburger et al., 2013). Also, during the dry season, there is a pronounced reduction of the mixing layer height in the north of South America caused by the North Atlantic Subtropical High-Pressure System, which minimizes the updrafts motion and hence vertical dispersion (Sanhueza et al., 1982). Additionally, biomass burning is higher during the dry season in Venezuela, mainly related to land-use change and agricultural activities, especially in the Venezuelan savannah region (Sanhueza et al., 1987). The effects of these events during the dry season are nationwide, with reported large aerosol

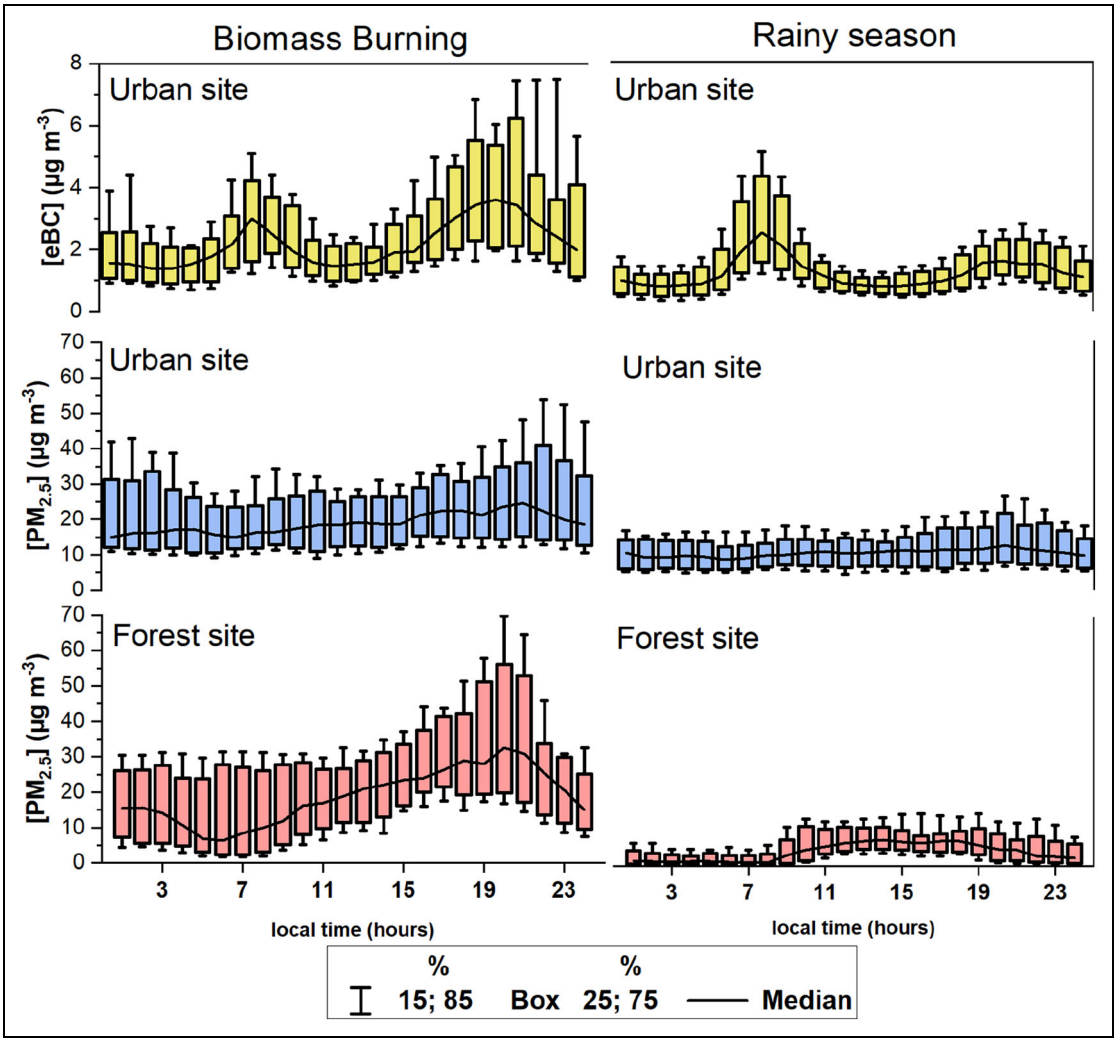


**Figure 5. Daily hour averages of eBC and $PM_{2.5}$ in µg $m^{-3}$ for the biomass burning period during the dry and rainy seasons, during the 7 days of the week.** Box border represents the 25th and 75th percentile, the gray whiskers represent the 15th and 85th percentile, and the line represents the median.

concentrations at a high-altitude remote station (4,765 m.a.s.l.) in the lower free troposphere of the Andes region in Venezuela (Hamburger et al., 2013).

In Caracas, during the dry season, mineral dust intrusions are typical (Saturno, 2013), as well as numerous forest fires in the mountains surrounding the valley, for example, Waraira Repano National Park (Morales et al., 1979). These events, together with the orography of the site and the reduction of the mixing layer height, can make the city experience significant pollution events during that period of the year (Guajardo et al., 2010). Therefore, we propose that the increase in aerosol concentration during the dry season results from different factors, including a reduction in the height of the mixing layer, the occurrence of mineral dust plumes, and the rise of biomass burning events.

The impact of traffic emissions on the diurnal cycle of eBC is present all year around. Nevertheless, eBC is also emitted during biomass burning episodes. Considering that the number of forest fires is commonly higher in Venezuela during the dry season, we decided to calculate the relative contribution of biomass burning to atmospheric eBC concentration. Different cases of eBC daily pattern concentrations in the urban site were compared, being these: The biomass burning period, the entire dry season, the dry season without biomass burning, and the rainy season (**Figure 7a–d**).

The eBC highest concentration peak was observed in the afternoons during the months with more biomass burning events in the dry season (**Figure 7a**). The median of eBC from 17:00 h to 22:00 h during the biomass burning period (**Figure 7a**) is higher (3.12 µg $m^{-3}$) compared with that found during the dry season without biomass burning (**Figure 7c**) (2.18 µg $m^{-3}$). The difference is directly attributed to the increase in biomass burning events. For the urban site, we estimated that biomass burning increases the eBC mass concentration by 30% during the dry season, indicating the importance of this source during this short period of the year. Factors contributing to this effect are less atmospheric washout and pronounced reduction in the mixed layer height in northern South America accentuated at the end of the day, increasing the air masses' residence time in the lower atmosphere (Sanhueza et al., 1982).

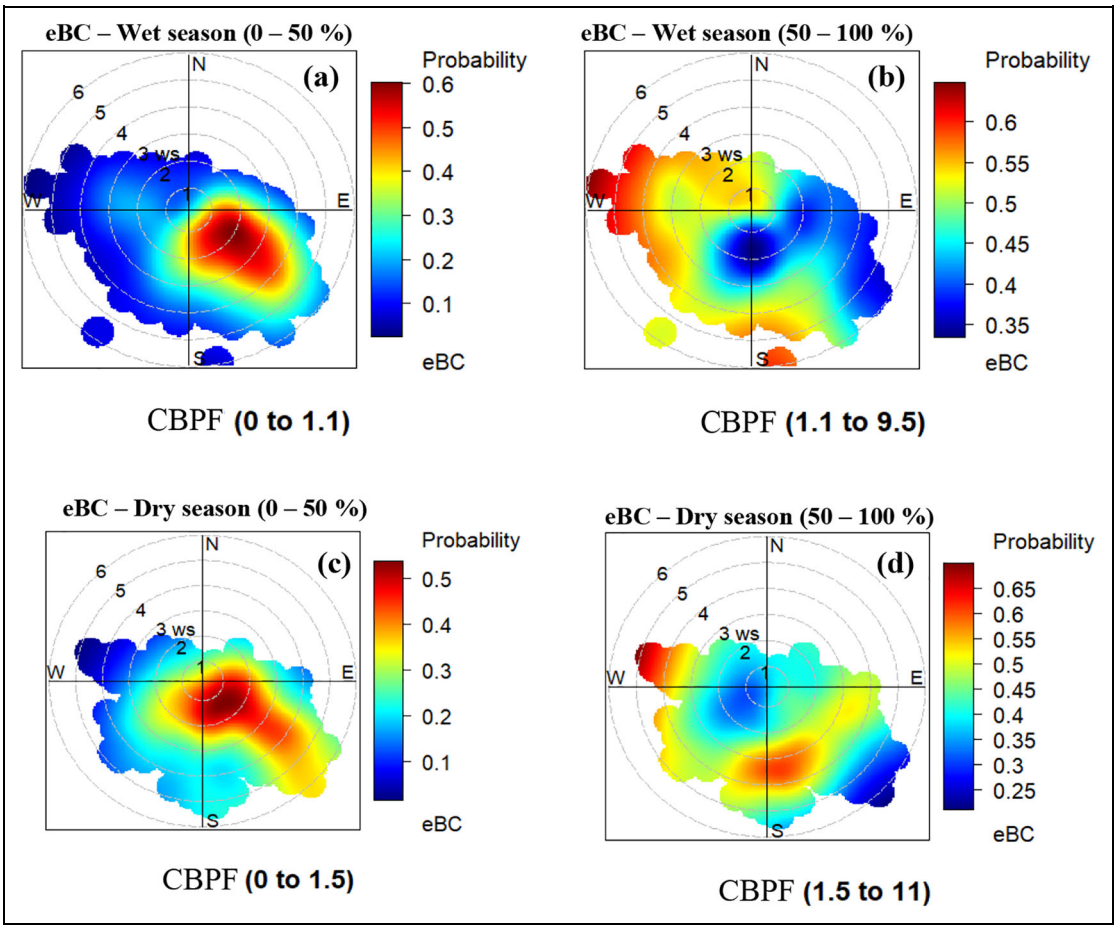


**Figure 6. Polar plots of the conditional bivariate probability function for percentile range 0–50, and 50–100, of the concentration of eBC in the urban site, during the wet and dry seasons, from medium hours.** The color scale represents the probability of finding a higher eBC. The circles reflect the wind speed in each wind direction vector.

On the other hand, the difference between the median of eBC from 17:00 h to 22:00 h for the rainy season (1.38 μg $m^{-3}$) with the one found during the dry season (2.70 μg $m^{-3}$) evidence that atmospheric washout reduces eBC concentration by 49%. Similar results are found when comparing the median eBC during the rainy season with the one observed during the biomass burning period. The first one is lower throughout the day, which shows the efficiency of atmospheric washing during this climatic period (**Figure 7b** and **d**). Assuming that the eBC concentration is exclusively from the burning of fossil fuels during the rainy season, the burning of biomass and the lack of atmospheric washout doubles the eBC concentration by 45% during the dry season. Such increment in eBC concentrations attributed to biomass burning could be translated into increments in the radiative forcing and impacts in the local climate, given the long residence time of eBC in the atmosphere.

### *4.4. Biomass burning events influence on high eBC and $PM_{2.5}$ concentrations*

To determine the influence of biomass burning on the eBC and $PM_{2.5}$ concentrations, we looked for correlations with specific fire events during the dry season (shown by the fire pixel counts for main biomass burning events in the north of Venezuela, Figure S4). We then explored 6 specific days (January 05, 2019, February 14, 2019, March 15, 2019, March 25, 2019, April 11, 2019, April 28, 2019), when daily mean concentrations were the largest observed ones in the entire campaign ($PM_{2.5}$ > 25 μg $m^{-3}$, and eBC > 7 μg $m^{-3}$) (**Figure 3**). Five out of 6 of those specific high concentration events selected showed back-trajectories crossing biomass burning events that featured paths over the urban and forest site. This result indicates that aerosols formed and emitted during such events could be transported to the monitoring sites by N–NE winds, increasing the mass concentration of eBC and $PM_{2.5}$ at the measurement sites (**Figures 8** and S5).

### *4.5. Contributing sources of eBC and $PM_{2.5}$*

We found 2 possible sources of eBC for the urban site during the wet season: (1) Nearby sources with relatively low eBC (0–1.1 μg $m^{-3}$), such as airplanes leaving and arriving at the Air Base derived from the wind speed (<5 m $s^{-1}$) that accompany them (CBPF percentiles 0–50th, **Figure 6**), and (2) sources from the northwest, southwest, and south, with relatively high eBC (1.1–9.5 μg $m^{-3}$) such as the Francisco Fajardo major freeway

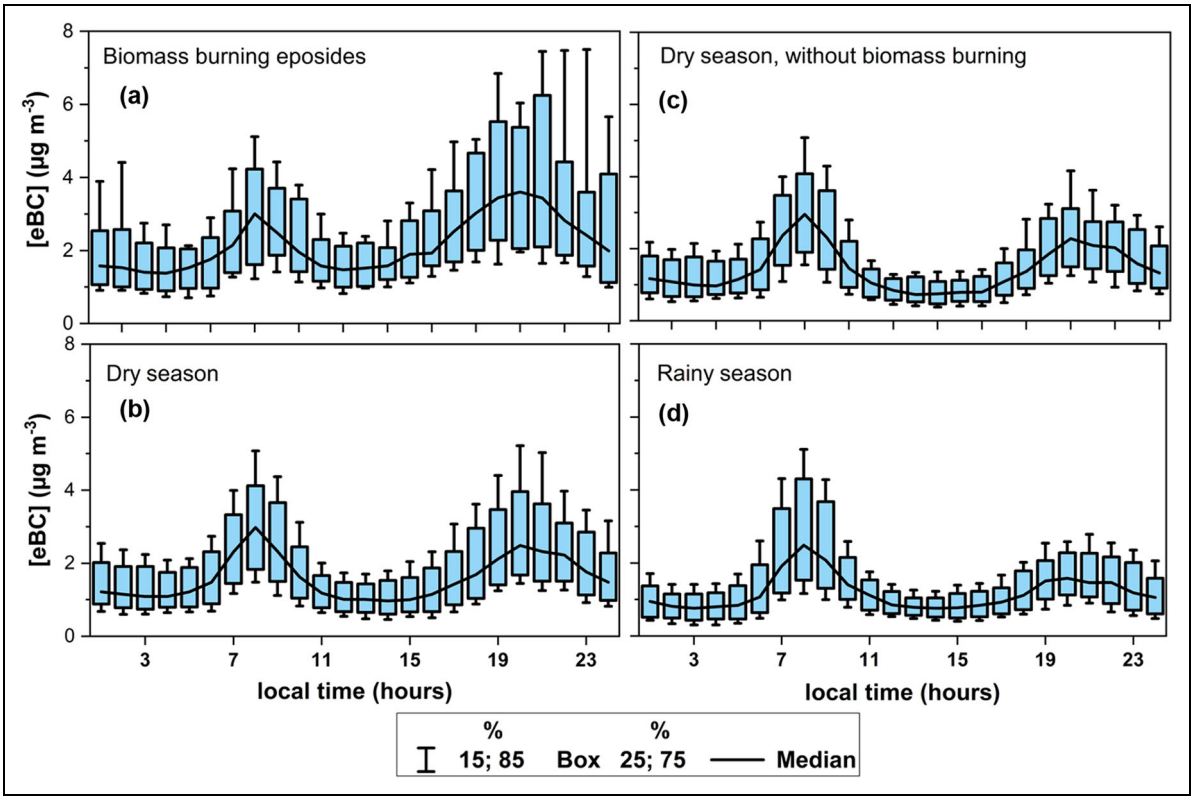


**Figure 7. Daily hour averages of eBC (µg m$^{-3}$) for (a) biomass burning period, (b) dry season, (c) dry season without biomass burning, and (d) rainy season during the 7 days of the week.** The box border represents the 25th and 75th percentile, the gray whiskers represent the 15th and 85th percentile, and the line represents the median.

(CBPF percentiles 50–100$^{th}$ **Figure 6a** and **b**). On the other hand, for low concentrations CBPF percentiles 0–50th during the dry season, the sources of eBC are similar to those observed during the wet season, while for high eBC concentrations (1.5–11 µg m$^{-3}$), they are spread between the northwest, southwest, south, and southeast for wind speed above 2 m s$^{-1}$ (**Figure 6c** and **d**). We analyze the occurrence of these concentrations more in detail and conclude that most of them happen during biomass burning events, discussed previously in Section 4.4.

Regarding $PM_{2.5}$ in the urban site during the wet season, the most likely nearby sources are the freeway mentioned above and residential sites for low concentrations ($\leq$13 µg m$^{-3}$) (Figure S2a and b). For higher $PM_{2.5}$ concentrations (13–80 µg m$^{-3}$) and wind speed >3 m s$^{-1}$ residential sites located in the south and southeast (Figure S2b). During the dry season, there is a specific contribution of $PM_{2.5}$ (0–9.7 µg m$^{-3}$) from the north and southeast. Still, for the highest concentrations range (9.7–114 µg m$^{-3}$), the sources are spread around the west, southwest, and southeast, where most of the biomass burning events take place (Figure S2c and d, see Section 4.4) and small industries in "La California" and "Petare" sectors are located. As seen for eBC, this is attributed to biomass burning events and is analyzed in Section 4.4.

For the forest site, which is located southwest from the urban site, the prevailing wind directions from north and northwest for all concentration ranges and CBPF percentiles indicate that the major contributor of $PM_{2.5}$ is the urban site during both the wet and dry seasons (Figure S3). $PM_{2.5}$ transport from the urban site may occur precisely during the first hours of the day when the mixing layer of the valley expands; then, air masses reach the forest site. The moderate contribution of $PM_{2.5}$ from sources located in the south of the forest site, with wind speeds in the range of 1–3 m s$^{-1}$, would indicate the influence of air masses from closer residential areas such as San Antonio de Los Altos and Los Teques. The highest concentrations observed during the dry season in the forest site, coming from the northeast and south sectors, are attributed to biomass burning events occurring throughout the mountainous area where the forest site is located at and the contribution of biomass burning events around the urban site.

### *4.6. Impact of increments in biomass burning events on regional air quality*

In South America, biomass burning events (forest fires and burning for agricultural purposes) contribute about 20% of global emissions from this source (e.g., Koch et al., 2009; van der Werf et al., 2010; Lee et al., 2018). However, limited information is available regarding the relative contribution of biomass burning during the dry period (November–April) from north of South America, but it is suggested to be large (Poveda et al., 2006; van der Werf et al., 2010; Thornhill et al., 2018).

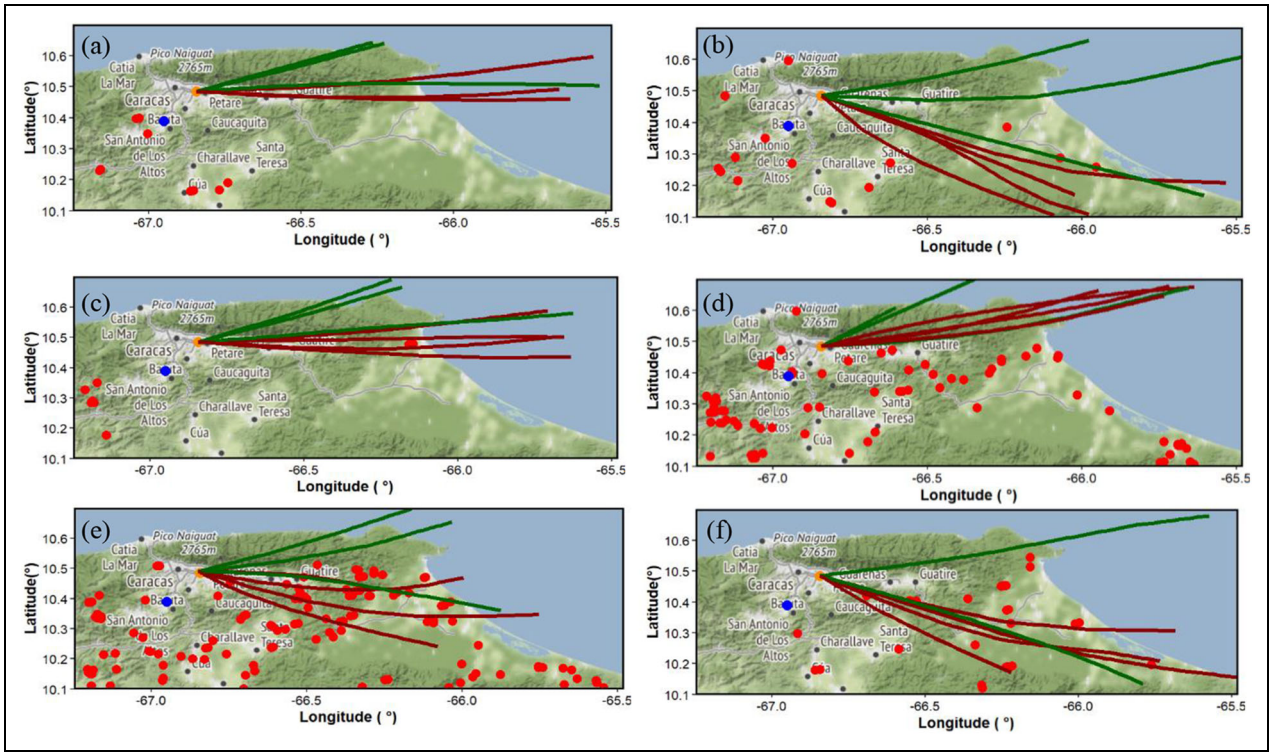


**Figure 8. Active fire locations (red dots) during 1-day backward trajectories arriving every 6 h at the urban site at 500 m (dark green) and 1,000 m (dark red) for (a) January 5, 2019, (b) February 14, 2019, (c) March 15, 2019, (d) March 25, 2019, (e) April 11, 2019, (f) April 28, 2019.** The blue dot is the forest site, and the yellow dot is the urban site.

The large increase of $PM_{2.5}$ and eBC average concentration during the dry season in Caracas (7% and 29%, respectively, compared to the annual average) is likely to have local and regional implications on air quality, as found elsewhere (Tsimpidi et al., 2016; Yadav and Devi, 2019). The impact on regional air quality occurs because the aerosols emitted during biomass burning are mainly fine particles that can be transported long distances, causing significant air pollution episodes far from the fires that generated them (Dejchanchaiwong et al., 2020).

A recent study suggests that the deterioration in the air quality during the dry season in densely populated areas of Bogota, Colombia occurs from a rise by up to 80% in aerosol concentration in the fine mode (Rincón-Riveros et al., 2020). Such particles are transported more than 1,000 km away after being emitted during biomass burning events in the Los Llanos region, the largest savannah area across northern South America (occupying western Venezuela and northeastern Colombia). Our study coincides with the time of measurements of Rincón-Riveros et al. (2020) during the dry season (January to April 2019). In their study, the concentrations of biomass burning tracers such as brown carbon, levoglucosan, $K^+$, and soluble organic carbon allow them to indicate that medium-range transport of biomass burning events during January 2019 causes an additional aerosol load of 15% ± 6%. Also, the monthly averages of $PM_{2.5}$, eBC, and brown carbon during February were 2, 5, and 8 times higher than that found in the month with the lowest concentration (July), respectively.

When comparing these results with ours, we infer that long-range transport of the biomass burning events that occur in the north of South America are likely to impact the air quality on a regional scale. The air masses charged with aerosols from biomass burning events reach the boundary layer, are transported long distances by the northern trade winds and can contribute to the aerosol load in long distance downwind areas. Proofs of this are as follows: (1) Enhancement of $PM_{2.5}$ concentrations in the planetary boundary layer during the dry season in the forest site (located at 1,400 m.a.s.l. and influenced by air masses from Caracas), as has been found in Guajardo et al. (2010); (2) eBC concentration nearly doubled during biomass burning events; and (3) biomass burning is responsible for 40% of the $PM_{2.5}$ increase (derived by eBC increase in Caracas during the same period).

The long-range transport of the fine aerosols from biomass burning in the north of South America can also increment the regional climate change. These aerosols can reach the Andean region and deposit on the snow surface, contributing to the melting of glaciers (Kang et al., 2020). For the first time for the north of South America, our results support that there is an influence of aerosol transport toward the Andean region through the movement of continental air masses, as has been previously inferred (Thornhill et al., 2018). For now, it is impossible to quantify this effect in the north of the Andean Cordillera. It would require black carbon measurements, snow cover, and runoff monitoring in the Andean region. Further continuous regional aerosol monitoring network and

modeling efforts will allow assessing the relative contribution of different sources and the impact on regional downwind air quality.

### 4.7. Estimates of the impact of biomass burning and its relationship with extreme events at the local level

It is expected an increase by 20%–50% in the number of days likely to cause extreme climate events, with sharper rises in the subtropical Southern Hemisphere (Bowman et al., 2017). Extreme climate events include heat waves, which create perfect conditions (reduction in rainfall and relative humidity, warmer air temperatures, vegetation drought) to increase the intensity and quantity of biomass burning events (Thornhill et al., 2018; Jones et al., 2020).

In recent decades, the proportion of extremely warm days doubled during December–January–February for Caracas (Feron et al., 2019). Therefore, positive climate feedback between heat waves and the occurrence of biomass burning might enhance their magnitude. In Caracas, for instance, an increase in the average temperature during the dry season would, at the same time, increase the probability of biomass burning events. These events emit and produce high concentrations of BC, which causes a positive radiative forcing 2,000 times greater than $CO_2$ on a molar basis (IPCC, 2021). Therefore, its positive feedback on the short-term regional climate will enhance the local warming, as observed in the Amazon (Liu, 2005).

By the middle of the 21st century, half or more of the days in December, January, and February could be scorching for northern South America if greenhouse gas and aerosol emissions continue increasing (Feron et al., 2019). The increase in the number of warm days would bring a higher number of biomass burning events, causing a rise of more than 2°C by 2040. The temperature rise would severely impact the global climate and biological diversity. The projections for Caracas indicate an increase of around 46% in extreme events (Feron et al., 2019). Therefore, continuous measurements of black carbon in Caracas and their correlation with the number of fires during the dry season are needed to establish empirical relationships, which should be incorporated in models for regional radiative forcing estimations and future heat waves projection.

### 4.8. El Nino—Southern Oscillation (ENSO) effects on $PM_{2.5}$ and BC concentrations

Coupled atmosphere-ocean interactions involve irregular, periodic variations in winds and sea surface temperatures during the ENSO, which affects the climate of much of the tropics and subtropics. ENSO modulates temperature and precipitation, impacting the PM variability at local and regional scales. Its effects in many sites are well documented, for example, in Asia and South America (Kim et al., 2013; Wie and Moon, 2017, Cai et al., 2020). Northeast South America and the Amazon are affected by severe drought during ENSO (Cai et al., 2020), which causes marked socio-economic, ecological, and environmental losses. For the period of measurements of this study, 2018–2019, the ENSO international dateline Index (ONI) was positive (0.5–0.9), corresponding to the El Niño phase (National Oceanic and Atmospheric Administration, n.d.). We only have 17 months of $PM_{2.5}$ and BC measurements for our study, and to capture a statistically significant ENSO effect in the regional atmospheric aerosol concentrations would require a more extended data set.

Although we cannot analyze the ENSO effect statistically, we infer that the large PM2.5 mean concentrations found in our study for both sites and BC in the urban site during the 2019 dry season related to biomass burning, could be in part caused by El Niño phase in Northeast South America. For instance, the 2015–2016 El Niño led to extreme drought conditions in northern South America, which, combined with elevated temperatures derived from global-warming trends, increased fire incidence by 36% compared with the preceding 12 years and pushed active fire detection beyond the agricultural transition zone (Cai et al., 2020). Consequently, $PM_{2.5}$ and BC concentrations are expected to increase proportionally compared to neutral conditions. For years when the ONI phase is neutral or negative, we could expect lower concentrations of $PM_{2.5}$ and BC, as has been observed in Colombia, for $PM_{2.5}$ concentrations (Arregocés et al., 2021).

### 4.9. $PM_{2.5}$ as air quality standard in Venezuela

Monitoring $PM_{2.5}$ can help policymakers reduce impacts on human health and air pollution and has been established as a mandatory air quality standard worldwide. Nevertheless, there are still no regulations for $PM_{2.5}$ in Venezuela, and total suspended particles is the only air quality standard in the country.

The $PM_{2.5}$ results obtained in both study sites were compared with the most recently updated limit values established by the World Health Organization (WHO) in 2021 (**Figure 3**). $PM_{2.5}$ annual averages from both measurement sites are above WHO's annual limit value (5 $\mu g\ m^{-3}$). In addition, the limit value (15 $\mu g\ m^{-3}$) of the 24-h average for $PM_{2.5}$ is exceeded during biomass burning events of the dry season (WHO, 2021), being for urban and forest sites $27 \pm 18\ \mu g\ m^{-3}$, and $28 \pm 21\ \mu g\ m^{-3}$, respectively.

Air quality regulation for $PM_{2.5}$ in Venezuela should be established, and this is of great relevance considering that both study sites experience air pollution episodes during the burning season bringing risks to the human health of the population. The $PM_{2.5}$ regulation becomes crucial considering that out of the most common diseases and injuries globally, upper respiratory infections have the most significant prevalence, incidence, years of living with disabilities, and high socioeconomical costs (Vos et al., 2016). In the meantime, mitigation strategies to minimize the effects in upper respiratory diseases and the potential asthmatic sequelae of exposure to biomass burning should be implemented during extreme events (D'Amato et al., 2015).

## 5. Conclusions

This work shows continuous measurements of $PM_{2.5}$ and eBC for the first time in the northernmost area of South America. We assessed the temporal variation and contributing sources of BC and $PM_{2.5}$ in Caracas, Venezuela. Evaluation of fire pixel maps with backward air masses trajectories showed that biomass burning events in the dry season is the major source of $PM_{2.5}$ and eBC at the urban and forest sites. The transport of air masses with large $PM_{2.5}$ and eBC concentrations from biomass burning events contributes to local and regional pollution. It also suggests a positive radiative forcing enhancement and, therefore, contribution to regional warming. The determined eBC concentrations from this study can be used for more accurate radiative forcing estimates from the north of South America and regional climate models.

Since biomass burning impacts the climate and air quality and, hence, human health, mitigation strategies to reduce the number of biomass burning events that have been increasing in recent years are imperative for the region. Also, international $PM_{2.5}$ daily limits are exceeded in both study sites during biomass burning episodes in the dry season, highlighting the importance of including $PM_{2.5}$ as an air quality standard in the country. $PM_{2.5}$ and eBC continuous measurements in Caracas and Altos de Pipe are recommended to develop further studies assessing their interannual variability and provide early warning systems to reduce health impacts for the population. Likewise, measurements of additional pollutants, such as $O_3$, sulfur dioxide, and nitrogen gases, among other atmospheric variables, would allow investigate the possible effects of natural oscillations in secondary aerosol formation and forecast changes in the local and regional air quality.

## Data accessibility statement

All data used in this article are publicly available in (https://owncloud.gwdg.de/index.php/s/cidoBjSXbN8u8xA).

## Supplemental files

The supplemental files for this article can be found as follows:

Figures S1–S5. Tables S1–S3. docx

## Acknowledgments

VE thanks all the Venezuelan Institute for Scientific Research (IVIC) technical staff and, in particular, Gregorio Maldonado for his assistance during the measurement campaign. We are deeply grateful to the Generalísimo Francisco de Miranda Air Base of the Bolivarian Military Aviation of Venezuela in Caracas for allowing us to place our urban site station in their base. Scientific advice, intellectual discussions, and lending of MAAP photometer from TROPOS institute are highly acknowledged. VE is grateful for the Ph.D. scholarship from IVIC.

## Funding

This work was supported by the Fondo Nacional de Ciencia, Tecnología e Innovación de Venezuela (FONACIT), Project No 2012-001679, and the European Commission funded Prediction of Air Pollution in Latin America and the Caribbean (PAPILA) project (No 777544).

## Competing interests

The authors declare that they have no conflict of interest.

## Author contributions

Contributed to conception and design: VE, TP, LD.
Contributed to acquisition and analysis of the data: VE.
Contributed to interpretation of data: VE, TP, LD.
Drafted and revised the article: VE, TP, LD.
Approved the submitted version for publication: VE, TP, LD, TM, AW.

## References

**Alas, HD**, **Müller, T**, **Birmili, W**, **Kecorius, S**, **Cambaliza, MO**, **Simpas, JBB**, **Cayetano, M**, **Weinhold, K**, **Vallar, E**, **Galvez, MC**, **Wiedensohler, A.** 2018. Spatial characterization of black carbon mass concentration in the atmosphere of a Southeast Asian megacity: An air quality case study for Metro Manila, Philippines. *Aerosol and Air Quality Research* **18**(9): 2301–2317. DOI: http://dx.doi.org/10.4209/aaqr.2017.08.0281.

**Amador-Muñoz, O**, **Villalobos-Pietrini, R**, **Miranda, J**, **Vera-Avila, LE.** 2011. Organic compounds of $PM_{2.5}$ in Mexico Valley: Spatial and temporal patterns, behavior and sources. *Science of the Total Environment* **409**(8): 1453–1465. DOI: http://dx.doi.org/10.1016/j.scitotenv.2010.11.026.

**Andrade-Flores, M**, **Rojas, N**, **Melamed, ML**, **Mayol-Bracero, OL**, **Grutter, M**, **Dawidowski, L**, **Antuña-Marrero, JC**, **Rudamas, C**, **Gallardo, L**, **Mamani-Paco, R**, **De Fatima Andrade, M, Huneeus, N.** 2016. Fostering a collaborative atmospheric chemistry research community in the Latin America and Caribbean region. *Bulletin of the American Meteorological Society* **97**(10): 1929–1939. DOI: http://dx.doi.org/10.1175/BAMS-D-14-00267.1.

**Andreae, MO.** 2001. The dark side of aerosols. *Nature* **409**(6821): 671–672. DOI: http://dx.doi.org/10.1038/35055640.

**Arregocés, H**, **Rojano, R**, **Restrepo, G.** 2021. El Niño southern oscillation (ENSO)-induced $PM_{10}$ variability in mining areas within the 2014–2017 period, Air pollution. *WIT Transactions on Ecology and the Environment* **252**: 213–222. DOI: http://dx.doi.org/10.2495/AIR210191.

**Artaxo, P**, **Martins, JV**, **Yamasoe, MA**, **Procópio, AS**, **Pauliquevis, TM**, **Andreae, MO**, **Guyon, P**, **Gatti, LV**, **Leal, AMC.** 2002. Physical and chemical properties of aerosols in the wet and dry seasons in Rondônia, Amazonia. *Journal of Geophysical Research: Atmospheres* **107**(20): 1–14. DOI: http://dx.doi.org/10.1029/2001JD000666.

**Aruna, K**, **Kumar, TVL**, **Rao, DN**, **Murthy, BVK**, **Babu, SS**, **Moorthy, KK.** 2013. Black carbon aerosols in a tropical semi-urban coastal environment: Effects of boundary layer dynamics and long range

transport. *Journal of Atmospheric and Solar-Terrestrial Physics* **104**(March 2011): 116–125. DOI: http://dx.doi.org/10.1016/j.jastp.2013.08.020.

**Backman, J**, **Rizzo, LV**, **Hakala, J**, **Nieminen, T**, **Manninen, HE**, **Morais, F**, **Aalto, PP**, **Siivola, E**, **Carbone, S**, **Hillamo, R**, **Artaxo, P**, **Virkkula, A**, **Petäjä, T**, **Kulmala, M.** 2012. On the diurnal cycle of urban aerosols, black carbon and the occurrence of new particle formation events in springtime São Paulo, Brazil. *Atmospheric Chemistry and Physics* **12**(23): 11733–11751. DOI: http://dx.doi.org/10.5194/acp-12-11733-2012.

**Begum, BA**, **Hopke, PK**, **Markwitz, A.** 2012. Air pollution by fine particulate matter in Bangladesh. *Atmospheric Pollution Research* **4**(1): 75–86. DOI: http://dx.doi.org/10.5094/apr.2013.008.

**Bogo, H**, **Otero, M**, **Castro, P**, **Ozafrán, MJ**, **Kreiner, A**, **Calvo, EJ**, **Negri, RM.** 2003. Study of atmospheric particulate matter in Buenos Aires city. *Atmospheric Environment* **37**(8): 1135–1147. DOI: http://dx.doi.org/10.1016/S1352-2310(02)00977-9.

**Bond, TC**, **Doherty, SJ**, **Fahey, DW**, **Forster, PM**, **Berntsen, T**, **DeAngelo, BJ**, **Flanner, MG**, **Ghan, S**, **Kärcher, B**, **Koch, D**, **Kinne, S**, **Kondo, Y**, **Quinn, PK**, **Sarofim, MC**, **Schultz, MG**, **Schulz, M**, **Venkataraman, C**, **Zhang, H**, **Zhang, S**, **Bellouin, N**, **Guttikunda, SK**, **Hopke, PK**, **Jacobson, MZ**, **Kaiser, JW**, **Klimont, Z**, **Lohmann, U**, **Schwarz, JP**, **Shindell, D**, **Storelvmo, T**, **Warren, S. G**, **Zender, CS.** 2013. Bounding the role of black carbon in the climate system: A scientific assessment. *Journal of Geophysical Research: Atmospheres* **118**: 5380–5552. DOI: http://dx.doi.org/10.1002/jgrd.50171.

**Bowman, DMJS**, **Williamson, GJ**, **Abatzoglou, JT**, **Kolden, CA**, **Cochrane, MA**, **Smith, AMS.** 2017. Human exposure and sensitivity to globally extreme wildfire events. *Nature Ecology and Evolution* **1**(3): 1–6. DOI: http://dx.doi.org/10.1038/s41559-016-0058.

**Bozlaker, A**, **Prospero, JM**, **Fraser, MP**, **Chellam, S**. 2013. Quantifying the contribution of long-range Saharan dust transport on particulate matter concentrations in Houston, Texas, using detailed elemental analysis. *Environmental Science & Technology* **47**(18): 10179–10187. DOI: http://dx.doi.org/10.1021/es4015663.

**Cai, Q**, **McPhaden, MJ**, **Grimm, AM**, **Rodrigues, RR**, **Taschetto, AS**, **Garreaud, RD**, **Dewitte, B**, **Poveda, G**, **Ham, Y**, **Santoso, A**, **Ng, B**, **Anderson, W**, **Wang, G**, **Geng, T**, **Jo, H**, **Marengo, JA**, **Alves, LM**, **Osman, M**, **Li, S**, **Wu, L**, **Karamperidou, C**, **Takahashi, K**, **Vera, C.** 2020. Climate impacts of the El Niño-Southern Oscillation on South America. *Nature Reviews Earth & Environment* **1**: 215–231. DOI: http://dx.doi.org/10.1038/s43017-020-0040-3.

**Chen, Y**, **Schleicher, N**, **Fricker, M**, **Cen, K**, **Liu, XL**, **Kaminski, U**, **Yu, Y**, **Wu, XF**, **Norra, S.** 2016. Long-term variation of black carbon and $PM_{2.5}$ in Beijing, China with respect to meteorological conditions and governmental measures. *Environmental Pollution* **212**: 269–278. DOI: http://dx.doi.org/10.1016/j.envpol.2016.01.008.

**Cheng, MT**, **Tsai, YI.** 2000. Characterization of visibility and atmospheric aerosols in urban, suburban, and remote areas. *Science of the Total Environment* **263**(1–3): 101–114. DOI: http://dx.doi.org/10.1016/S0048-9697(00)00670-7.

**Cheng, Z**, **Luo, L**, **Wang, S**, **Wang, Y**, **Sharma, S**, **Shimadera, H**, **Wang, X**, **Bressi, M**, **De Miranda, RM**, **Jiang, J**, **Zhou, W**, **Fajardo, O**, **Yan, N**, **Hao, J.** 2016. Status and characteristics of ambient $PM_{2.5}$ pollution in global megacities. *Environment International* **89–90**: 212–221. DOI: http://dx.doi.org/10.1016/j.envint.2016.02.003.

**Chow, JC**, **Watson, JG**, **Park, K**, **Lowenthal, DH**, **Robinson, NF**, **Park, K**, **Maglian, KA.** 2006. Comparison of particle light scattering and fine particulate matter mass in central California. *Journal of the Air and Waste Management Association* **56**(4): 398–410. DOI: http://dx.doi.org/10.1080/10473289.2006.10464515.

**Cohen, DD**, **Stelcer, E**, **Santos, FL**, **Prior, M**, **Thompson, C**, **Pabroa, PCB.** 2009. Fingerprinting and source apportionment of fine particle pollution in Manila by IBA and PMF techniques: A 7-year study. *X-Ray Spectrometry* **38**(1): 18–25. DOI: http://dx.doi.org/10.1002/xrs.1112.

**Colarco, PR**, **Toon, OB**, **Reid, JS**, **Livingston, JM**, **Russel, P.B**, **Redemann, J**, **Schmid, B**, **Maring, HB**, **Savoei, D**, **Welton, EJ**, **Campbell, JR**, **Holben, BN**, **Levy, R.** 2003. Saharan dust transport to the Caribbean during PRIDE: 2. Transport, vertical profiles, and deposition in simulations of in situ and remote sensing observations. *Journal of Geophysical Research* **108**(D19): 1–16. DOI: http://dx.doi.org/10.1029/2002jd002659.

**Cuenca, HG.** 1987. Los mecanismos de tolerancia al aluminio de la vegetación del bosque tropical nublado que crece sobre suelos ácidos [M.Sc. thesis]. Caracas, Venezuela: Instituto Venezolano de Investigaciones Científicas.

**D'Amato, G**, **Holgate, ST**, **Pawankar, R**, **Ledford, DK**, **Cecchi, L**, **Al-Ahmad, M**, **Al-Enezi, F**, **Al-Muhsen, S**, **Ansotegui, I**, **Baena-Cagnani, CE**, **Baker, DJ**, **Bayram, H**, **Bergmann, KC**, **Boulet, LP**, **Buters, JTM**, **D'Amato, M**, **Dorsano, S**, **Douwes, J**, **Finlay, SE**, **Garrasi, D**, **Gómez, M**, **Haahtela, T**, **Halwani, R**, **Hassani, Y**, **Mahboub, B**, **Marks, G**, **Michelozzi, P**, **Montagni, M**, **Nunes, C**, **Jae-Won Oh, J**, **A Popov, T**, **Portnoy, J**, **Ridolo, E**, **Rosário, N**, **Rottem, M**, **Sánchez-Borges, M**, **Sibanda, E**, **Sienra-Monge, JJ**, **Vitale, C**, **Annesi-Maesano, I.** 2015. Meteorological conditions, climate change, new emerging factors, and asthma and related allergic disorders. A statement of the World Allergy Organization. *World Allergy Organization Journal* **8**(1): 1–52. DOI: http://dx.doi.org/10.1186/s40413-015-0073-0.

**Dejchanchaiwong, R**, **Tekasakul, P**, **Tekasakul, S**, **Phairuang, W**, **Nim, N**, **Sresawasd, C**, **Thongboon, K**,

**Thongyen, T**, **Suwattiga, P**. 2020. Impact of transport of fine and ultrafine particles from open biomass burning on air quality during 2019 Bangkok haze episode. *Journal of Environmental Sciences* **97**: 149–161. DOI: http://dx.doi.org/10.1016/j.jes.2020.04.009.

**Draxler, RR**, **Hess, GD.** 1988. An overview of the HYSPLIT 4 modeling system for trajectories, dispersion, and deposition. *Australian Meteorological Magazine* **47**: 295–308.

**Feron, S**, **Cordero, RR**, **Damiani, A**, **Llanillo, PJ**, **Jorquera, J**, **Sepulveda, E**, **Asencia, V**, **Laroze, D**, **Carrasco, J**, **Torres, G**. 2019. Observations and projections of heat waves in South America. *Scientific Reports* **9**: 8173. DOI: http://dx.doi.org/10.1038/s41598-019-44614-4.

**Figueroa, DA**, **Rodríguez-Sierra, CJ**, **Jiménez-Velez, BD.** 2006. Concentrations of Ni and V, other heavy metals, arsenic, elemental and organic carbon in atmospheric fine particles ($PM_{2.5}$) from Puerto Rico. *Toxicology and Industrial Health* **22**(2): 87–99. DOI: http://dx.doi.org/10.1191/0748233706th247oa.

**Finlayson-Pitts, B**, **Pitts, J**, **Jr.** 2000. *Chemistry of the upper and lower atmosphere*. San Diego, CA: Academic Press.

**Gaw Report No. 227**. 2016. *WMO/GAW aerosol measurement procedures, guidelines, and recommendations*. 2nd Edition. Geneva, Switzerland: World Meteorological Organization. Available at https://library.wmo.int/doc_num.php?explnum_id=3073. Accessed May 1, 2022.

**Gioda, A**, **Amaral, BS**, **Monteiro, ILG**, **'Pierre, STD**. 2011. Chemical composition, sources, solubility, and transport of aerosol trace elements in a tropical region. *Journal of Environmental Monitoring* **13**(8): 2134–2142. DOI: http://dx.doi.org/10.1039/c1em10240 k, 2011.

**Guajardo, N**, **Ramírez, A**, **Díaz, F**, **Castillo, E**, **Otero, A**, **Parra, J.** 2010. Concentración de las partículas totales suspendidas en la atmósfera de Caracas [Concentration of total suspended particles in the atmosphere of Caracas]. *Revista de la Facultad de Ingeniería de la UCV* [*Journal of the School of Engineering from Universidad Central de Venezuela*] **25**(2): 81–91.

**Hamburger, T**, **Matisans, M**, **Tunved, P**, **Stroem, J**, **Calderon, S**, **Hoffmann, P**, **Hochschild, G**, **Gross, J**, **Schmeissner, T**, **Wiedensohler, A**, **Krejci, R.** 2013. Long-term in situ observations of biomass burning aerosol at a high-altitude station in Venezuela—Sources, impacts and interannual variability. *Atmospheric Chemistry and Physics* **13**: 9837–9853. DOI: http://dx.doi.org/10.5194/acp-13-9837-2013.

**Haywood, J.** 2021. Atmospheric aerosols and their role in climate change, in Elsevier, BV ed., *Climate change*: 645–659. DOI: http://dx.doi.org/10.1016/b978-0-12-821575-3.00030-x.

**Hsu, YM**, **Wang, X**, **Chow, JC**, **Watson, JG**, **Percy, KE.** 2016. Collocated comparisons of continuous and filter-based $PM_{2.5}$ measurements at Fort McMurray, Alberta, Canada. *Journal of the Air and Waste Management Association* **66**(3): 329–339. DOI: http://dx.doi.org/10.1080/10962247.2015.1136362.

**Instituto Nacional de Estadística**. 2012. Informe Geoambiental 2011, Gerencia de estadísticas ambientales, República Bolivariana de Venezuela. Available at https://web.archive.org/web/20121009164814/http://www.ine.gov.ve/documentos/Demografia/CensodePoblacionyVivienda/pdf/distrito_capital.pdf. Accessed October 16, 2020.

**Instituto Nacional de Transporte Terrestre**. 2013. Anuario estadístico del Instituto Nacional de Transporte Terrestre. Caracas, Venezuela: Ministerio del Poder Popular Para Relaciones Interiores, Justicia y Paz.

**Intergovernmental Panel on Climate Change**. 2021. Climate change 2021: The physical science basis (Masson-Delmotte, V, Zhai, P, Pirani, A, Connors, SL, Péan, C, Berger, S, Caud, N, Chen, Y, Goldfarb, L, Gomis, MI, Huang, M, Leitzell, K, Lonnoy, E, Matthews JBR, Maycock, TK, Waterfield, T, Yelekçi, O, Yu, R, and Zhou, B eds.). *Contribution of Working Group I to the Sixth Assessment Report of the Intergovernmental Panel on Climate Change.* Cambridge, UK: Cambridge University Press.

**Jaklevic, JM**, **Gatti, RC**, **Goulding, FS**, **Loo, BW.** 1981. A β-gauge method applied to aerosol samples. *Environmental Science & Technology* **15**(6): 680–686. DOI: http://dx.doi.org/10.1021/es00088a006.

**Ježek, I**, **Katrašnik, T**, **Westerdahl, D**, **Mocnik, G.** 2015. Black carbon, particle number concentration and nitrogen oxide emission factors of random in-use vehicles measured with the on-road chasing method. *Atmospheric Chemistry and Physics* **15**(19): 11011–11026. DOI: http://dx.doi.org/10.5194/acp-15-11011-2015.

**Jones, MW**, **Smith, A**, **Betts, R**, **Canadell, JG**, **Prentice, IC**, **Le Quéré, C**. 2020. Climate change increases the risk of wildfires. *ScienceBrief Review*. Available at https://sciencebrief.org/briefs/wildfires. Accessed August 2, 2021.

**Kabatas, B**, **Unal, A**, **Pierce, RB**, **Kindap, T, Pozzoli, L.** 2014. The contribution of Saharan dust in $PM_{10}$ concentration levels in Anatolian Peninsula of Turkey. *Science of the Total Environment* **488–489**(1): 413–421. DOI: http://dx.doi.org/10.1016/j.scitotenv.2013.12.045.

**Kang, S**, **Zhang, Y**, **Qian, Y**, **Wang, HA**. 2020. Review of black carbon in snow and ice and its impact on the cryosphere. *Earth-Science Reviews* **210**: 103346. DOI: http://dx.doi.org/10.1016/j.earscirev.2020.103346.

**Kassomenos, PA**, **Vardoulakis, S**, **Chaloulakou, A**, **Paschalidou, AK**, **Grivas, G**, **Borge, R**, **Lumbreras, J**. 2014. Study of $PM_{10}$ and $PM_{2.5}$ levels in three European cities: Analysis of intra and inter urban variations. *Atmospheric Environment* **87**: 153–163. DOI: http://dx.doi.org/10.1016/j.atmosenv.2014.01.004.

**Kim, JS**, **Zhou, W**, **Cheung, H**, **Chow, C.** 2013. Variability and risk analysis of Hong Kong air quality based on

Monsoon and El Niño conditions. *Advances in Atmospheric Sciences* **30**: 280–290. DOI: http://dx.doi.org/10.1007/s00376-012-2074-z.

**Koch, D**, **Schulz, M**, **Kinne, S**, **Mcnaughton, C**, **Spackman, JR**, **Balkanski, Y**, **Bauer, S**, **Berntsen, T**, **Bond, TC**, **Boucher, O**, **Chin, M**, **Clarke, A**, **De Luca, N**, **Dentener, F**, **Diehl, T**, **Dubovik, O**, **Easter, R**, **Fahey, DW**, **Feichter, J**, **Fillmore, D**, **Freitag, S**, **Ghan, S**, **Ginoux, P**, **Gong, S**, **Horowitz, L**, **Iversen, T**, **Kirkevag, A**, **Klimont, Z**, **Kondo, Y**, **Krol, M**, **Liu, X**, **Miller, R**, **Montanaro, V**, **Moteki, N**, **Myhre, G**, **Penner, JE**, **Perlwitz, J**, **Pitari, G**, **Reddy, S**, **Sahu, L**, **Sakamoto, H**, **Schuster, G**, **Schwarz, JP**, **Seland, O**, **Stier, P**, **Takegawa, N**, **Takemura, T**, **Textor, C**, **Van Aardenne, JA**, **Zhao, Y.** 2009. Evaluation of black carbon estimations in global aerosol models. *Atmospheric Chemistry and Physics* **9**: 9001–9026. DOI: http://dx.doi.org/10.5194/acp-9-9001-2009.

**Koutrakis, P**, **Sax, SN**, **Sarnat, JA**, **Coull, B**, **Demokritou, P**, **Oyola, P**, **Garcia, J**, **Gramsch, E**. 2005. Analysis of $PM_{10}$, $PM_{2.5}$, and $PM_{2.5–10}$ concentrations in Santiago, Chile, from 1989 to 2001. *Journal of the Air and Waste Management Association* **55**(3): 342–351. DOI: http://dx.doi.org/10.1080/10473289.2005.10464627.

**Kulkarni, P**, **Baron, PA**, **Willeke, K**. 2011. *Aerosol measurement principles, techniques, and applications*. 3rd Edition. Hoboken, NJ: Wiley.

**Kumar, KR**, **Narasimhulu, K**, **Balakrishnaiah, G**, **Reddy, BSK**, **Gopal, KR**, **Reddy, RR**, **Satheesh, SK**, **Moorthy, KK**, **Babu, SS.** 2011. Characterization of aerosol black carbon over a tropical semi-arid region of Anantapur, India. *Atmospheric Research* **100**(1): 12–27. DOI: http://dx.doi.org/10.1016/j.atmosres.2010.12.009.

**Kutlar Joss, M**, **Eeftens, M**, **Gintowt, E**, **Kappeler, R**, **Künzli, N**. 2017. Time to harmonize national ambient air quality standards. *International Journal of Public Health* **62**(4): 453–462. DOI: http://dx.doi.org/10.1007/s00038-017-0952-y.

**Landrigan, PJ**, **Fuller, R**, **Acosta, NJR**, **Adeyi, O**, **Arnold, R**, **Basu, N**, **(Nil), Baldé, AB**, **Bertollini, R**, **Bose-O'Reilly, S**, **Boufford, JI**, **Breysse, PN**, **Chiles, T**, **Mahidol, C**, **Coll-Seck, AM**, **Cropper, ML**, **Fobil, J**, **Fuster, V**, **Greenstone, M**, **Haines, A**, **Hanrahan, D**, **Hunter, D**, **Khare, M**, **Krupnick, A**, **Lanphear, B**, **Lohani, B**, **Martin, K**, **Mathiasen, KV**, **McTeer, MA**, **Murray, C. JL**, **Ndahimananjara, JD**, **Perera, F**, **Potočnik, J**, **Preker, AS**, **Ramesh, J**, **Rockström, J**, **Salinas, C**, **Samson, LD**, **Sandilya, K**, **Sly, PD**, **Smith, KR**, **Steiner, A**, **Stewart, RB**, **Suk, WA**, **Van Schayck, OCP**, **Yadama, GN**, **Yumkella, K**, **Zhong, M**. 2018. The lancet commission on pollution and health. *The Lancet* **391**(10119): 462–512. DOI: http://dx.doi.org/10.1016/S0140-6736(17)32345-0.

**Latha, KM**, **Badarinath, KVS**. 2005a. Seasonal variations of $PM_{10}$ and $PM_{2.5}$ particles loading over tropical urban environment. *International Journal of Environmental Health Research* **15**(1): 63–68. DOI: http://dx.doi.org/10.1080/09603120400018964.

**Latha, KM**, **Badarinath, KVS**. 2005b. Seasonal variations of black carbon aerosols and total aerosol mass concentrations over urban environment in India. *Atmospheric Environment* **39**(22): 4129–4141. DOI: http://dx.doi.org/10.1016/j.atmosenv.2005.04.004.

**Lee, H-H**, **Iraqui, O**, **Gu, Y**, **Yim, SH-L**, **Chulakadabba, A**, **Tonks, AY-M**, **Yang, Z**, **Wang, C**. 2018. Impacts of air pollutants from fire and non-fire emissions on the regional air quality in Southeast Asia. *Atmospheric Chemistry and Physics* **18**: 6141–6156. DOI: http://dx.doi.org/10.5194/acp-18-6141-2018.

**Liu, Y**. 2005. Atmospheric response and feedback to radiative forcing from biomass burning in tropical South America. *Agricultural and Forest Meteorology* **133**: 40–53. DOI: http://dx.doi.org/10.1016/j.agrformet.2005.03.

**Liu, L**, **Bei, N**, **Hu, B**, **Wu, J**, **Liu, S**, **Li, X**, **Wang, R**, **Liu, Z**, **Shen, Z**, **Li, G**. 2020. Wintertime nitrate formation pathways in the north China plain: Importance of $N_2O_5$ heterogeneous hydrolysis. *Environmental Pollution* **266**. DOI: http://dx.doi.org/10.1016/j.envpol.2020.115287.

**Liu, Q**, **Ma, T**, **Olson, MR**, **Liu, Y**, **Zhang, T**, **Wu, Y**, **Schauer, JJ**. 2016. Temporal variations of black carbon during haze and non-haze days in Beijing. *Scientific Reports* **6**: 1–10. DOI: http://dx.doi.org/10.1038/srep33331.

**Liu, T**, **He, Q**, **Chen, Y**, **Liu, J**, **Liu, Q**, **Fu, X**, **Zhang, J**, **Huang, G**, **Li, R**. 2021. Distinct impacts of humidity profiles on physical properties and secondary formation of aerosols in Shanghai. *Atmospheric Environment* **267**(September): 118756. DOI: http://dx.doi.org/10.1016/j.atmosenv.2021.118756.

**Liu, Z**, **Hu, B**, **Wang, L**, **Wu, F**, **Gao, W**, **Wang, Y**. 2014. Seasonal and diurnal variation in particulate matter ($PM_{10}$ and $PM_{2.5}$) at an urban site of Beijing: Analyses from a 9-year study. *Environmental Science and Pollution Research* **22**(1): 627–642. DOI: http://dx.doi.org/10.1007/s11356-014-3347-0.

**Mariani, RL**, **De Mello, WZ**. 2007. $PM_{2.5-10}$, $PM_{2.5}$ and associated water-soluble inorganic species at a coastal urban site in the metropolitan region of Rio de Janeiro. *Atmospheric Environment* **41**(13): 2887–2892. DOI: http//dx.doi.org/10.1016/j.atmosenv.2006.12.009.

**Martins Pereira, G**, **Teinilä, K**, **Custódio, D**, **Gomes Santos, A**, **Xian, H**, **Hillamo, R**, **Alves, CA**, **Andrade, BDJ**, **Rocha, ODG**, **Kumar, P**, **Balasubramanian, R**, **Andrade, DFM**, **Vasconcellos, PDC**. 2017. Particulate pollutants in the Brazilian city of Saõ Paulo: 1-year investigation for the chemical composition and source apportionment. *Atmospheric Chemistry and Physics* **17**(19): 11943–11969. DOI: http//dx.doi.org/10.5194/acp-17-11943-2017.

**Ministerio del Ambiente y Recursos Naturales**. 1995. Decreto 638 (Ordinance 638). Normas sobre calidad del aire y control de la contaminación atmosférica [Air quality standards and control of air pollution], Gaceta oficial N° 4.899. Caracas, Venezuela: Gobierno Bolivariano de Venezuela.

**Moosmüller, H**, **Chakrabarty, RK**, **Arnott, WP**. 2009. Aerosol light absorption and its measurement: A review. *Journal of Quantitative Spectroscopy and Radiative Transfer* **110**(11): 844–878. DOI: http//dx.doi.org/10.1016/j.jqsrt.2009.02.035.

**Morales, J**, **Cano, Y**, **Sánchez, L**, **Torres, J**, **Stanislao, I**. 2012. Evaluación preliminar de los niveles de partículas atmosféricas $PM_{10}$ y $PM_{2,5}$ en la ciudad de Maracaibo, Venezuela. *Multiciencias* **12**(2): 156–161.

**Morales, JA**, **Escalona, L**, **Ishizaki, C**, **Sanhueza, E**. 1979. Forest Fires: An important source of benzo (a) Pyrene in the Caracas valley forest fires: An important source of benzo (a) Pyrene in the Caracas Valley. *Journal of the Air Pollution Control Association* **29**(10): 1072–1073. DOI: http//dx.doi.org/10.1080/00022470.1979.10470900.

**Morantes, G**, **González, JC**, **Rincón, G**. 2021. Characterisation of particulate matter and identification of emission sources in Greater Caracas, Venezuela. *Air Quality, Atmosphere and Health* **14**(0123456789): 1989–2014. DOI: http//dx.doi.org/10.1007/s11869-021-01070-2.

**Moran-Zuloaga, D**, **Ditas, F**, **Walter, D**, **Saturno, J**, **Brito, J**, **Carbone, S**, **Chi, X**, **Hrabě De Angelis, I**, **Baars, H**, **Godoi, HMR**, **Heese, B**, **Holanda, AB**, **Lavrič, JV**, **Martin, S**, **Ming, J**, **Pöhlker, LM**, **Ruckteschler, N**, **Su, H**, **Wang, Y**, **Wang, Q**, **Wang, Z**, **Weber, B**, **Wolff, S**, **Artaxo, P**, **Pöschl, U**, **Andreae, M**, **Pöhlker, C**. 2018. Long-term study on coarse mode aerosols in the Amazon rain forest with the frequent intrusion of Saharan dust plumes. *Atmospheric Chemistry and Physics* **18**(13): 10055–10088. DOI: http//dx.doi.org/10.5194/acp-18-10055-2018.

**Müller, T**, **Henzing, JS**, **De Leeuw, G**, **Wiedensohler, A**, **Alastuey, A**, **Angelov, H**, **Bizjak, M**, **Collaud Coen, M**, **Engström, JE**, **Gruening, C**, **Hillamo, R**, **Hoffer, A**, **Imre, K**, **Ivanow, P**, **Jennings, G**, **Sun, JY**, **Kalivitis, N**, **Karlsson, H**, **Komppula, M**, **Laj, P**, **Li, S-M**, **Lunder, C**, **Marinoni, A**, **Martins dos Santos, S**, **Moerman, M**, **Nowak, A**, **Ogren, JA**, **Petzold, A**, **Pichon, JM**, **Rodriquez, S**, **Sharma, S**, **Sheridan, PJ**, **Teinilä, K**, **Tuch, T**, **Viana, M**, **Virkkula, A**, **Weingartner, E**, **Wilhelm, R**, **Wang, YQ**. 2011. Characterization and intercomparison of aerosol absorption photometers: Result of two intercomparison workshops. *Atmospheric Measurement Techniques* **4**: 245–268. DOI: http//dx.doi.org/10.5194/amt-4-245-2011.

**National Oceanic and Atmospheric Administration**. n.d. National Weather Service, National Centers for Environmental Prediction, Climate Prediction Center, 5830 University Research Court, College Park, Maryland 20740, Page Author: Climate Prediction Center Internet Team. Available at https://origin.cpc.ncep.noaa.gov/products/analysis_monitoring/ensostuff/ONI_v5.php. Accessed May 10, 2022.

**Paralovo, SL**, **Barbosa, CGG**, **Carneiro, IPS**, **Kurzlop, P**, **Borillo, GC**, **Schiochet, MFC**, **Godoi, AFL**, **Yamamoto, CI**, **de Souza, RAF**, **Andreoli, RV**, **Ribeiro, IO**, **Manzi, AO**, **Kourtchev, I**, **Bustillos, JOV**, **Martin, ST**, **Godoi, RHM**. 2019. Observations of particulate matter, $NO_2$, $SO_2$, $O_3$, $H_2S$ and selected VOCs at a semi-urban environment in the Amazon region. *Science of the Total Environment* **650**(2): 996–1006. DOI: http//dx.doi.org/10.1016/j.scitotenv.2018.09.073.

**Patel, MM**, **Chillrud, SN**, **Correa, JC**, **Feinberg, M**, **Hazi, Y**, **Deepti, KC**, **Prakash, S**, **Ross, JM**, **Levy, D**, **Kinney, PL**. 2009. Spatial and temporal variations in traffic-related particulate matter at New York City high schools. *Atmospheric Environment* **43**(32): 4975–4981. DOI: http//dx.doi.org/10.1016/j.atmosenv.2009.07.004.

**Petzold, A**, **Ogren, JA**, **Fiebig, M**, **Laj, P**, **Li, SM**, **Baltensperger, U**, **Holzer-Popp, T**, **Kinne, S**, **Pappalardo, G**, **Sugimoto, N**, **Wehrli, C**, **Wiedensohler, A**, **Zhang, XY**. 2013. Recommendations for reporting black carbon measurements. *Atmospheric Chemistry and Physics* **13**(16): 8365–8379. DOI: http//dx.doi.org/10.5194/acp-13-8365-2013.

**Petzold, A**, **Schloesser, H**, **Sheridan, PJ**, **Arnott, WP**, **Ogren, JA**, **Virkkula, A**. 2005. Evaluation of multiangle absorption photometry for measuring aerosol light absorption. *Aerosol Science and Technology* **39**(1): 40–51. DOI: http//dx.doi.org/10.1080/027868290901945.

**Petzold, A**, **Schönlinner, M**. 2004. Multi-angle absorption photometry - A new method for the measurement of aerosol light absorption and atmospheric black carbon. *Journal of Aerosol Science* **35**(4): 421–441. DOI: http//dx.doi.org/10.1016/j.jaerosci.2003.09.005.

**Poveda, G**, **Waylen, RR**, **Pulwarty, RS**. 2006. Annual and inter-annual variability of the present climate in northern South America and southern Mesoamerica. *Palaeogeography, Palaeoclimatology, Palaeoecology* **234**(1): 3–27. DOI: http//dx.doi.org/10.1016/j.palaeo.2005.10.031.

**Prospero, JM**, **Glaccum, RA**, **Nees, RT**. 1981. Atmospheric transport of soil dust from Africa to South America. *Nature* **289**: 570–572. DOI: http//dx.doi.org/10.1038/289570a0.

**Prospero, JM**, **Mayol-Bracero, OL**. 2013. Understanding the transport and impact of African dust on the Caribbean Basin. *Bulletin of the American Meteorological Society* **94**(9): 1329–1337. DOI: http//dx.doi.org/10.1175/BAMS-D-12-00142.1.

**Ramírez, O**. 2014. Intrusiones de polvo africano en la región Caribe de Colombia [African dust intrusions in the Caribbean region of Colombia]. *Gestión y Ambiente* **17**(2): 11–29.

**Resquin, MD**, **Santágata, D**, **Gallardo, L**, **Gómez, D**, **Rössler, C**, **Dawidowski, L**. 2018. Local and remote black carbon sources in the Metropolitan Area of Buenos Aires. *Atmospheric Environment* **182**(November 2017): 105–114. DOI: http//dx.doi.org/10.1016/j.atmosenv.2018.03.018.

**Retama, A**, **Baumgardner, D**, **Raga, GB**, **McMeeking, GR**, **Walker, JW**. 2015. Seasonal and diurnal trends

in black carbon properties and co-pollutants in Mexico City. *Atmospheric Chemistry and Physics* **15**(16): 9693–9709. DOI: http//dx.doi.org/10.5194/acp-15-9693-2015.

**Rincón-Riveros, JM**, **Rincón-Caro, MA**, **Sullivan, AP**, **Mendez-Espinosa, JF**, **Belalcazar, LC**, **Quirama Aguilar, M**, **Morales Betancourt, R**. 2020. Long-term brown carbon and smoke tracer observations in Bogotá, Colombia: Association with medium-range transport of biomass burning plumes. *Atmospheric Chemistry and Physics* **20**: 7459–7472. DOI: http//dx.doi.org/10.5194/acp-20-7459-2020.

**Riojas-Rodriguez, H**, **da Silva, AS**, **Texcalac-Sangrador, JLJL**, **Moreno-Banda, GL**, **Riojas-Rodríguez, H**, **da Silva, AS**, **Texcalac-Sangrador, JLJL**, **Moreno-Banda, GL**. 2016. Air pollution management and control in Latin America and the Caribbean: Implications for climate change. *Revista Panamericana de Salud Pública* **40**(3): 150–159. Available at http://iris.paho.org/xmlui/handle/123456789/31229.

**Safai, PD**, **Kewat, S**, **Praveen, PS**, **Rao, PSP**, **Momin, GA**, **Ali, K**, **Devara, PCS**. 2007. Seasonal variation of black carbon aerosols over a tropical urban city of Pune, India. *Atmospheric Environment* **41**(13): 2699–2709. DOI: http//dx.doi.org/10.1016/j.atmosenv.2006.11.044.

**Sahu, LK**, **Kondo, Y**, **Miyazaki, Y**, **Pongkiatkul, P**, **Kim Oanh, NT**. 2011. Seasonal and diurnal variations of black carbon and organic carbon aerosols in Bangkok. *Journal of Geophysical Research: Atmospheres* **116**(15): 1–14. DOI: http//dx.doi.org/10.1029/2010JD015563.

**Salvador, P**, **Almeida, SM**, **Cardoso, J**, **Almeida-Silva, M**, **Nunes, T**, **Cerqueira, M**, **Alves, C**, **Reis, MA**, **Chaves, PC**, **Artíñano, B**, **Pio, C**. 2016. *Composition and origin of $PM_{10}$ in Cape Verde: Characterization of long-range transport episodes*. Amsterdam, the Netherlands: Elsevier Ltd.

**Sanhueza, E**. 2002. Un recuento de los estudios de química atmosférica en el bosque nublado de Altos de Pipe (IVIC). Contribución al conocimiento de la ecología, química ambiental y otros aspectos importantes del bosque nublado de Altos de Pipe, Venezuela. Instituto Venezolano de Investigaciones Científicas (IVIC), Centro de Ecología, Altos de Pipe, Venezuela.

**Sanhueza, E**, **Africano, M**, **Romero, J**. 1982. Air pollution in tropical áreas. *Science of the Total Environment* **23**: 3–10. DOI: http//dx.doi.org/ 10.1016/0048-9697(82)90115-2.

**Sanhueza, E**, **Fernández, E**, **Donoso, L**, **Romero, J**. 2000. Boundary layer ozone in the tropical America northern hemisphere region. *Journal of Atmospheric Chemistry* **35**(3): 249–272. DOI: http//dx.doi.org/10.1023/A:1006270911796.

**Sanhueza, E**, **Rondón, A**, **Romero, J**. 1987. Airborne particles in the Venezuelan savannah during burning and non-burning periods. *Atmospheric Environment* **21**(10): 2227–2231. DOI: http//dx.doi.org/10.1016/0004-6981(87)90354-4.

**Saturno, J**. 2013 Jan. Carbono negro atmosférico en áreas con distintos niveles de actividades antrópicas [M.Sc. thesis]. Caracas, Venezuela: Instituto Venezolano de Investigaciones Científicas.

**Seinfeld, JH**, **Pandis, SN**. 1998. *From air pollution to climate change. Atmospheric chemistry and physics*. New York, NY: John Wiley and Sons.

**Sena, A**. 2003. Determinación de los factores que intervienen en los procesos fotoquímicos en la atmósfera de Caracas [M.Sc. thesis]. Caracas, Venezuela: Universidad Central de Venezuela.

**Schmeissner, T**, **Krejci, R**, **Ström, J**, **Birmili, W**, **Wiedensohler, A**, **Hochschild, G**, **Gross, J**, **Hoffmann, P**, **Calderon, S**. 2011. Analysis of number size distributions of tropical free tropospheric aerosol particles observed at Pico Espejo (4765 ma.s.l.), Venezuela. *Atmospheric Chemistry and Physics* **11**: 3319–3332. DOI: http//dx.doi.org/10.5194/acp-11-3319-2011.

**Shrivastava, M**, **Lou, S**, **Zelenyuk, A**, **Easter, RC**, **Corley, RA**, **Thrall, BD**, **Rasch, PJ**, **Fast, JD**, **Simonich, SLM**, **Shen, H**, **Tao, S**. 2017. Global long-range transport and lung cancer risk from polycyclic aromatic hydrocarbons shielded by coatings of organic aerosol. *Proceedings of the National Academy of Sciences USA* **114**(6): 1246–1251. DOI: http//dx.doi.org/10.1073/pnas.1618475114.

**Silva, J**, **Rojas, J**, **Norabuena, M**, **Molina, C**, **Toro, RA**, **Leiva-Guzmán, MA**. 2017. Particulate matter levels in a South American megacity: The metropolitan area of Lima-Callao, Peru. *Environmental Monitoring and Assessment* **189**(12): 635. DOI: http//dx.doi.org/10.1007/s10661-017-6327-2.

**Slowik, JG**, **Cross, ES**, **Han, JH**, **Davidovits, P**, **Onasch, TB**, **Jayne, JT**, **Williams, LR**, **Canagaratna, MR**, **Worsnop, DR**, **Chakrabarty, RK**, **Moosmüller, H**, **Arnott, WP**, **Schwarz, JP**, **Gao, RS**, **Fahey, DW**, **Kok, GL**, **Petzold, A**. 2007. An inter-comparison of instruments measuring black carbon content of soot particles. *Aerosol Science and Technology* **41**(3): 295–314. DOI: http//dx.doi.org/10.1080/02786820701197078.

**Suárez-Salas, L**, **Álvarez Tolentino, D**, **Bendezú, Y**, **Pomalaya, J**. 2017. Caracterización Química Del Material Particulado Atmosférico Del Centro Urbano De Huancayo, Perú. *Revista de la Sociedad Química del Perú* **83**(2): 187–199. DOI: http//dx.doi.org/10.37761/rsqp.v83i2.197.

**Swap, R**, **Garstang, M**, **Greco, S**. 1992. Saharan dust in the Amazon Basin. *Tellus* **44**(B): 133–149. DOI: http//dx.doi.org/ 10.3402/tellusb.v44i2.15434.

**Thomas, A**, **Gebhart, J**. 1994. Correlations between gravimetry and light scattering photometry for atmospheric aerosols. *Atmospheric Environment* **28**(5): 935–938. DOI: http//dx.doi.org/10.1016/1352-2310(94)90251-8.

**Thornhill, GD**, **Ryder, CL**, **Highwood, EJ**, **Shaffrey, LC**, **Johnson, BT**. 2018. The effect of South American biomass burning aerosol emissions on the regional climate. *Atmospheric Chemistry and Physics* **18**:

5321–5342. DOI: http//dx.doi.org/10.5194/acp-18-5321-2018.

**Tiwari, S**, **Srivastava, AK**, **Bisht, DS**, **Parmita, P**, **Srivastava, MK**, **Attri, SD**. 2013. Diurnal and seasonal variations of black carbon and $PM_{2.5}$ over New Delhi, India: Influence of meteorology. *Atmospheric Research* **125–126**: 50–62. DOI: http//dx.doi.org/10.1016/j.atmosres.2013.01.011.

**Tsimpidi, AP**, **Karydis, VA**, **Pandis, SN**, **Lelieveld, J**. 2016. Global combustion sources of organic aerosols: Model comparison with 84 AMS factor-analysis data sets. *Atmospheric Chemistry and Physics* **16**: 8939–8962. DOI: http//dx.doi.org/10.5194/acp-16-8939-2016.

**UNEP, CCAC**. 2018. *Integrated assessment of short-lived climate pollutants in Latin America and the Caribbean: Improving air quality while contributing to climate change mitigation*. ISBN: 978-92-807-3549-9.

**Uria-Tellaetxe, I**, **Carslaw, DC**. 2014. Conditional bivariate probability function for source identification. *Environmental Modelling & Software* **59**: 1–9. DOI: http//dx.doi.org/10.1016/j.envsoft.2014.05.002.

**van der Werf, GR**, **Randerson, JT**, **Giglio, L**, **Collatz, GJ**, **Mu, M**, **Kasibhatla, PS**, **Morton, DC**, **DeFries, RS**, **Jin, Y**, **van Leeuwen, TT**. 2010. Global fire emissions and the contribution of deforestation, savanna, forest, agricultural, and peat fires (1997–2009). *Atmospheric Chemistry and Physics* **10**: 11707–11735. DOI: http//dx.doi.org/10.5194/acp-10-11707-2010.

**Venkataraman, C**, **Habib, G**, **Eiguren-Fernandez, A**, **Miguel, AH**, **Friedlander, SK**. 2005. Residential biofuels in South Asia: Carbonaceous aerosol emissions and climate impacts. *Science* **307**(5714): 1454–1456. DOI: http//dx.doi.org/10.1126/science.1104359.

**Verma, S**, **Pani, SK**, **Bhanja, SN**. 2013. Sources and radiative effects of wintertime black carbon aerosols in an urban atmosphere in east India. *Chemosphere* **90**(2): 260–269. DOI: http//dx.doi.org/10.1016/j.chemosphere.2012.06.063.

**Vos, T**, **Allen, C**, **Arora, M**, **Barber, RM**, **Brown, A**, **Carter, A**, **Casey, DC**, **Charlson, FJ**, **Chen, AZ**, **Coggeshall, M**, **Cornaby, L**, **Dandona, L**, **Dicker, DJ**, **Dilegge, T**, **Erskine, HE**, **Ferrari, AJ**, **Fitzmaurice, C**, **Fleming, T**, **Forouzanfar, MH**, **Zuhlke, LJ**. 2016. Global, regional, and national incidence, prevalence, and years lived with disability for 310 diseases and injuries, 1990–2015: A systematic analysis for the Global Burden of Disease Study 2015. *The Lancet* **388**(10053): 1545–1602. DOI: http//dx.doi.org/10.1016/S0140-6736(16)31678-6.

**Wang, S**, **Yu, J**, **Okubo, K**. 2019. Scenario analysis on the generation of end-of-life hybrid vehicle in developing countries—Focusing on the exported secondhand hybrid vehicle from Japan to Mongolia. *Recycling* **4**(4): 41. DOI: http//dx.doi.org/10.3390/recycling4040041.

**Wang, X**, **Chancellor, G**, **Evenstad, J**, **Farnsworth, JE**, **Hase, A**, **Olson, GM**, **Sreenath, A**, **Agarwal, JK**. 2009. A novel optical instrument for estimating size segregated aerosol mass concentration in real-time. *Aerosol Science and Technology* **43**(9): 939–950. DOI: http//dx.doi.org/10.1080/02786820903045141.

**Wang, Y**, **Yeo, GT**. 2016. A study on international multimodal transport networks from Korea to central Asia: Focus on secondhand vehicles. *The Asian Journal of Shipping and Logistics* **32**(1): 41–47. DOI: http//dx.doi.org/10.1016/j.ajsl.2016.03.005.

**Wie, J**, **Moon, B**. 2017. ENSO-related PM10 variability on the Korean Peninsula. *Atmospheric Environment* **167**: 426–433. DOI: https://dx.doi.org/10.1016/j.atmosenv.2017.08.052.

**World Health Organization**. 2021. *Global air quality guidelines: Particulate matter ($PM_{2.5}$ and $PM_{10}$), ozone, nitrogen dioxide, sulfur dioxide, and carbon monoxide*. World Health Organization. Available at https://apps.who.int/iris/handle/10665/345329. Accessed December 18, 2021.

**Yadav, IC**, **Devi, NL**. 2019. Biomass burning, regional air quality, and climate change. *Encyclopedia of Environmental Health*: 386–391. DOI: https://dx.doi.org/10.1016/B978-0-12-409548-9.11022-X.

**Zhu, T**, **Melamed, M**, **Parrish, D**, **Gauss, M**, **Klenner, LG**, **Lawrence, M**. 2012. WMO/IGAC impacts of megacities on air pollution and climate. GAW Report No. 205, World Meteorological Organization, Geneva. WMO/IGAC Impacts of megacities on air pollution and climate, Vol. **1**; ISBN 9780988286702.

**How to cite this article:** Engelhardt, V, Pérez, T, Donoso, L, Müller, T, Wiedensohler, A. 2022. Black carbon and particulate matter mass concentrations in the Metropolitan District of Caracas, Venezuela: An assessment of temporal variation and contributing sources. *Elementa: Science of the Anthropocene* 10(1). DOI: https://doi.org/10.1525/elementa.2022.00024

**Domain Editor-in-Chief:** Detlev Helmig, Boulder AIR LLC, Boulder, CO, USA

**Associate Editor:** Balram Ambade, Department of Chemistry, National Institute of Technology, Jamshedpur, India

**Knowledge Domain:** Atmospheric Science

**Published:** August 26, 2022 **Accepted:** June 29, 2022 **Submitted:** February 10, 2022



ELEMENTA Science of the Anthropocene

*Elem Sci Anth* is a peer-reviewed open access journal published by University of California Press.

OPEN ACCESS